Generated using the official AMS LaTeX template v6.1

# Coupled Stratospheric Ozone and Atlantic Meridional Overturning Circulation Feedbacks on the Northern Hemisphere Midlatitude Jet Response to $4xCO_2$

Clara Orbe[a,b] , David Rind[a] , Darryn Waugh[c] , Jeffrey Jonas[a,d] , Xiyue Zhang[c] , Gabriel Chiodo[e] , Larissa Nazarenko[a,d] , and Gavin A. Schmidt[a]

[a] *NASA Goddard Institute for Space Studies, New York, NY*

[b] *Department of Applied Physics and Applied Mathematics, Columbia University, New York, NY*

[c] *Department of Earth and Planetary Sciences, Johns Hopkins University, Baltimore, MD*

[d] *Center for Climate Systems Research, Earth Institute, Columbia University, New York, NY*

[e] *Institute for Atmospheric and Climate Science, ETH Zurich, Switzerland*

*Corresponding author*: Clara Orbe, clara.orbe@nasa.gov

ABSTRACT: Stratospheric ozone, and its response to anthropogenic forcings, provide an important pathway for the coupling between atmospheric composition and climate. In addition to stratospheric ozone's radiative impacts, recent studies have shown that changes in the ozone layer due to 4x$CO_2$ have a considerable impact on the Northern Hemisphere (NH) tropospheric circulation, inducing an equatorward shift of the North Atlantic jet during boreal winter. Using simulations produced with the NASA Goddard Institute for Space Studies (GISS) high-top climate model (E2.2) we show that this equatorward shift of the Atlantic jet can induce a more rapid weakening of the Atlantic Meridional Overturning Circulation (AMOC). The weaker AMOC, in turn, results in an eastward acceleration and poleward shift of the Atlantic and Pacific jets, respectively, on longer timescales. As such, coupled feedbacks from both stratospheric ozone and the AMOC result in a two-timescale response of the NH midlatitude jet to abrupt 4x$CO_2$ forcing: a "fast" response (5-20 years) during which it shifts equatorward and a "total" response ($\sim$100-150 years) during which the jet accelerates and shifts poleward. The latter is driven by a weakening of the AMOC that develops in response to weaker surface zonal winds, that result in reduced heat fluxes out of the subpolar gyre and reduced North Atlantic Deep Water formation. Our results suggest that stratospheric ozone changes in the lower stratosphere can have a surprisingly powerful effect on the AMOC, independent of other aspects of climate change.

## 1. Introduction

There is large uncertainty in the atmospheric circulation response to increasing greenhouse gases (see Shepherd (2014) and references therein). Although models generally predict a poleward shift of the midlatitude eddy-driven jet, the magnitude of this shift is highly uncertain (e.g., Vallis et al. (2015); Grise and Polvani (2014)) as are its underlying drivers (Shaw (2019)). This is especially true in the Northern Hemisphere (NH), where there are opposing thermodynamic influences, i.e. opposite meridional temperature gradient responses at the surface versus the upper troposphere (Shaw et al. (2016)). Thus, while enhanced warming in the lower polar troposphere relative to the lower tropical troposphere (i.e., Arctic amplification) contributes to reduced meridional temperature gradients, increases in upper tropospheric tropical warming contribute to enhanced temperature gradients aloft (Butler et al. (2010); Yuval and Kaspi (2020)) and it is not clear how these competing processes affect the zonal mean midlatitude jet.

Many processes have been shown to influence the response of meridional temperature gradients to increased $CO_2$, including polar amplification (see Smith et al. (2019) and references therein) and cloud feedbacks (e.g., Ceppi and Hartmann (2015); Voigt and Shaw (2015)). By comparison, composition feedbacks associated with the ozone response to $CO_2$ have been less well examined although stratospheric ozone changes have been identified as an important pathway coupling composition to climate (Isaksen et al. (2009)). In particular, the stratospheric ozone response to $4xCO_2$ consists of robust decreases in the tropical lower stratosphere (LS), increases in the tropical upper stratosphere and increases over high latitudes (Chiodo et al. (2018)). In the tropics, the reductions in LS ozone are strongly correlated with the response of stratospheric upwelling (Fig. 6 in Chiodo et al. (2018)) and, while the exact details of these changes are model dependent, especially over high latitudes, the general pattern is very consistent among models (e.g., Nowack et al. (2015); Chiodo et al. (2018) and Chiodo and Polvani (2019) (hereafter CP2019)).

This pattern of reduced (increased) ozone over the tropical (high latitude) LS in response to $4xCO_2$ has immediate implications for temperature gradients in the stratosphere by cooling the tropics and warming high latitudes (Nowack et al. (2015); Chiodo et al. (2018); Li and Newman (2022)). As CP2019 and Li and Newman (2022) showed, these changes in temperature gradients drive an anomalous equatorward shift of the midlatitude jet in the Southern Hemisphere (SH). In addition, both studies also showed shifts in the Northern Hemisphere (NH) during boreal winter, where anomalies extend down into the lower troposphere and are concentrated over the Atlantic, resembling the negative phase of the North Atlantic Oscillation (NAO). By comparison, ozone feedbacks on LS temperature gradients do not result in a robust response of the Pacific jet (CP2019).

A more recent study by Zhang et al. (2023) that considered two models – distinct from the ones used in either CP2019 or Li and Newman (2022) – and that differed only in their representation of interactive chemistry, also showed that changes in composition can impact the sign of the NH midlatitude jet response to increased $CO_2$. However, in contrast to CP2019, the long-term impact of this composition feedback was a *poleward*, not equatorward, shift of the zonal mean NH jet. Though not investigated in detail, this poleward shift of the jet – expressed regionally as an eastward extension of the Atlantic jet and a poleward shift of the Pacific jet – was linked to changes in the ocean circulation, which were not examined in CP2019. More precisely, Zhang et al. (2023) noted that the Atlantic Meridional Overturning Circulation (AMOC) exhibited a stronger decline in interactive simulations in which trace gases and aerosols were allowed to respond to increased $CO_2$, relative to non-interactive simulations. Indeed, recent studies have highlighted the large influence that changes in the AMOC exert on the response of the NH midlatitude jet to increased $CO_2$ (Gervais et al. (2019)), with models featuring a larger AMOC decline also tending to produce a stronger and eastward extended jet over the Atlantic (Bellomo et al. (2021); Liu et al. (2020); Orbe et al. (2023)).

The results from Zhang et al. (2023) suggest that composition feedbacks on the NH midlatitude jet may depend on the response of the ocean circulation. However, that study did not examine the mechanism underlying the stronger AMOC response in the interactive chemistry simulations nor did it isolate the role of ozone from influences due to other trace gases and aerosols. To this end, here we hypothesize that the ozone-induced negative NAO wind anomalies reported in CP2019 provide a potential pathway through which stratospheric ozone changes can influence the AMOC and the long-term response of the NH midlatitude jet. Our hypothesis is partly predicated on results from previous studies showing that variations in the jet – namely those resembling the NAO – can influence variability of the AMOC through changes in wind stress (Marshall et al. (2001); Zhai et al. (2014); Delworth and Zeng (2016)). Modified air-sea fluxes of heat, water and momentum associated with variations in the NAO alter vertical and horizontal density gradients in the subpolar gyre, inducing changes in deep water formation and the AMOC (e.g., Visbeck et al. (1998); Delworth and Dixon (2000)). This pathway via the NAO has been used to demonstrate how sudden stratospheric warmings influence the variability of heat flux anomalies into the ocean and ocean mixed layer depths in the North Atlantic (O'Callaghan et al. (2014)) as well as the strength of the AMOC itself (Reichler et al. (2012)).

Here we present results from non-interactive and fully interactive chemistry global warming experiments produced with the new high-top coupled atmosphere ocean version of the NASA Goddard Institute for Space Studies (GISS) climate model that were submitted to the Coupled Model Intercomparison Project Phase 6 (CMIP6) (Eyring et al. (2016)). We focus on simulations in which $CO_2$ is abruptly doubled and quadrupled in order to facilitate comparison with the results presented in CP2019 and Zhang et al. (2023).

We begin by verifying that reduced ozone in the tropical lower stratosphere, which is captured only in the interactive simulations, leads to an equatorward shift of the midlatitude jet on relatively fast timescales. Then we show that the AMOC response in the interactive simulations is largely associated with these ozone-driven changes in the jet, not aerosols, using new experiments in which the stratospheric ozone response to $4xCO_2$ is isolated from changes in other trace gases and aerosols. In particular, we show that our model captures the ozone-induced negative NAO-like pattern first reported in CP2019; in addition, we also find that ozone-driven changes in surface friction speed further weaken the AMOC, resulting in a long-term poleward shift of the NH jet. As a result, we show that both stratospheric ozone changes and the AMOC influence the NH jet on distinct "fast" and "total" timescales (and in the opposite sense), comprising a coupled atmosphere-ocean feedback on the NH midlatitude jet response to increased $CO_2$. While the former "fast" feedback was documented in CP2019, the latter has, to the best of our knowledge, not been reported in previous studies.

We begin by discussing methods in Section 2 and then present key results and conclusions in Sections 3 and 4, respectively.

## 2. Methods

### *a. Model and Configurations*

Here we use the NASA Goddard Institute for Space Studies (GISS) "Middle Atmosphere (MA)" Model E2.2 (Rind et al. (2020); Orbe et al. (2020)). E2.2 consists of 102 vertical levels spanning the surface up to 0.002 hPa and is run at a horizontal resolution of 2 degrees by 2.5 degrees. Orographic and non-orographic gravity wave drag is parameterized following Lindzen (1987) and Rind et al. (1988), producing in E2.2 a quasibiennial oscillation (QBO) that compares well with observations as well as improved stratospheric polar vortex variability (Ayarzagüena et al. (2020); Rind et al. (2020)). Of most relevance to this study, Orbe et al. (2020) showed that E2.2 produces a significantly improved representation of the Brewer-Dobson and stratospheric transport circulations, compared to the lower vertical resolution CMIP6 version of ModelE (E2.1, Kelley et al. (2020)), resulting in reduced biases in ozone, methane, water vapor and nitrous oxide (see their Figure 1). Among the different model versions discussed in Rind et al. (2020) and Orbe et al. (2020) here we focus on the "Altered-Physics" (-AP) Version (E2.2-AP) because this is the configuration that was submitted to CMIP6 and presented in recent studies (Ayarzagüena et al. (2020); DallaSanta et al. (2021a,b)).

We begin by showing the results reported in Zhang et al. (2023) using both "Non-INTeractive" (NINT) (Table 1, rows 1-3) and fully interactive "One-Moment Aerosols" (OMA) (Bauer et al. (2020); Table 1, rows 4-6) configurations. In the NINT configuration all trace gases and aerosols are set to preindustrial values. Hence, in the 2- and 4x$CO_2$ NINT runs neither ozone nor other trace gases (besides water vapor) change in response to increased $CO_2$. By comparison, the OMA 2- and 4x$CO_2$ runs capture the full ozone response to $CO_2$, as well as composition feedbacks associated with other trace gases and aerosols.

In order to isolate the role of ozone feedbacks on the circulation, we then perform experiments using a linearized ozone (LINOZ) configuration (Table 1, rows 7-9). In LINOZ the stratospheric ozone field is calculated interactively by Taylor expanding the equation of state around present-day (2000–2010) values such that the ozone tendency is, to first-order, parameterized as a function of the local ozone mixing ratio, temperature, and overhead column ozone (McLinden et al. (2000)). Tropospheric ozone is calculated using monthly mean ozone production and loss rates archived

TABLE 1. The Model E2.2 experiments presented in this study, including preindustrial control, abrupt 2x$CO_2$ and abrupt 4x$CO_2$ simulations using NINT (rows 1-3), OMA (rows 4-6) and LINOZ (rows 7-9) configurations. Four NINT abrupt 4x$CO_2$ ensemble members are included (row 3) in order to compare with a four member 4x$CO_2$ ensemble produced using the LINOZ configuration (row 9). The 4x$CO_2$ ensemble mean LINOZ ozone response is also used to force four prescribed SST and SIC preindustrial experiments (row 10) in which all forcings other than ozone are set to preindustrial values. All coupled atmosphere-ocean simulations are run using the GISS Ocean v1 (GO1) (i.e., "-G" in CMIP6 notation).

| Configuration | Ozone | $CO_2$ | Ensemble Size | SSTs and SICs |
|---|---|---|---|---|
| NINT | Preindustrial | Preindustrial | 1 | coupled (-G ocean) |
| NINT | Preindustrial | 2x$CO_2$ | 1 | coupled (-G ocean) |
| NINT | Preindustrial | 4x$CO_2$ | 4 | coupled (-G ocean) |
| OMA | Preindustrial | Preindustrial | 1 | coupled (-G ocean) |
| OMA | 2x$CO_2$ | 2x$CO_2$ | 1 | coupled (-G ocean) |
| OMA | 4x$CO_2$ | 4x$CO_2$ | 1 | coupled (-G ocean) |
| LINOZ | Preindustrial | Preindustrial | 1 | coupled (-G ocean) |
| LINOZ | 2x$CO_2$ | 2x$CO_2$ | 1 | coupled (-G ocean) |
| LINOZ | 4x$CO_2$ | 4x$CO_2$ | 4 | coupled (-G ocean) |
| NINT | LINOZ 4x$CO_2$ | Preindustrial | 4 | Prescribed Preindustrial |

from GEOS-CHEM (Rind et al. (2014)). In contrast to NINT, therefore, the LINOZ ensemble captures the influence of the ozone response to $CO_2$ on the large-scale circulation. Unlike OMA, however, it is much more computationally efficient to run and isolates the ozone feedback from feedbacks related to other trace gases and aerosols. DallaSanta et al. (2021a) previously showed that the LINOZ ozone parameterization reproduces well the vertical structure and seasonal cycle of stratospheric ozone obtained from the fully interactive OMA configuration (see their Figure 1).

### *b. Experiments*

For the different model configurations (NINT, OMA, LINOZ) we perform 150-year-long abrupt 2- and 4x$CO_2$ experiments, in which $CO_2$ values are abruptly doubled and quadrupled relative to preindustrial concentrations. For each model configuration, these experiments are branched from a corresponding preindustrial control simulation. For NINT and LINOZ four-member 4x$CO_2$ ensembles are run in order to assess the robustness of any ozone feedbacks. These experiments are all conducted using the atmosphere-ocean version of E2.2-AP that is coupled to the GISS Ocean v1 (GO1) (i.e., "-G" in CMIP6 notation, hereafter simply E2.2-G). For coupled atmosphere-ocean configurations in which (four-member) ensembles are run, different ensemble members are chosen from different initial ocean states spaced 20 years apart in the corresponding preindustrial control simulation.

In addition to the coupled atmosphere-ocean experiments, we also present results from a four-member ensemble of 60-year-long atmosphere-only experiments in which sea surface temperatures (SSTs) and sea ice concentrations (SICs) are fixed to preindustrial values, but the monthly mean time-evolving ensemble mean ozone response from the coupled LINOZ 4x$CO_2$ experiments is prescribed (Table 1, row 10). This allows us to quantify the impact of the ozone feedback represented in LINOZ on the large-scale circulation, absent any contributions from changes in background $CO_2$, sea ice concentrations or sea surface temperatures.

### *c. Analysis*

#### 1) Timescales

When examining the midlatitude jet response to increased $CO_2$ we account for the fact that extratropical circulation changes consist of distinct "fast" and "slow" responses (Ceppi et al. (2018), hereafter CZS2018). More precisely, CZS2018 show that most of the shift of the midlatitude jets occurs within 5-10 years of a steplike (abrupt) $CO_2$ forcing, with little shifts occurring during a slower response over which SSTs change over subsequent decades. In contrast to the Southern Hemisphere, zonal asymmetries play an important role in the Northern Hemisphere, where the influence of local patterns in sea surface temperature change can result in oppositely signed jet shifts between the Pacific and Atlantic ocean basins on "slow" timescales. Given this potential for compensating jet shifts on distinct timescales, we therefore decompose the $CO_2$ circulation response into "fast" and "total" timescale responses.

More precisely, we modify the original approach used in CZS2018 to define our "fast" response as the difference between the ensemble mean 4x$CO_2$ response, averaged over years 5-20 (as opposed to years 5-10), and the corresponding preindustrial control simulation. Calculations of the "fast" response using years 5-10 produce similar results (not shown), but the choice of years 5-20 better accounts for the large internal variability in our runs, perhaps related to a somewhat larger ENSO amplitude in our model compared to observations (Rind et al. (2020)).

In addition, instead of focusing on the "slow" response, defined in CZS2018 as the difference between averages over years 121-140 and years 5-10, here we examine the "total" response, defined as the difference between the ensemble mean 4x$CO_2$ response, averaged over years 100-150, and the preindustrial control simulation. This approach for defining the "total" response is not only more consistent with what was used in Zhang et al. (2023) and CP2019, with which we directly compare our results throughout, but also with numerous other studies examining the atmospheric circulation response to an abrupt quadrupling of $CO_2$ (e.g., Grise and Polvani (2014, 2016); Menzel et al. (2019)). Note that in response to an abrupt quadrupling of $CO_2$ the NINT model configuration produces global mean surface temperature "fast" and "total" responses of ~2.9°C and ~3.9°C, respectively.

Statistical significance of the four-member ensemble mean LINOZ-NINT and single member OMA-NINT abrupt $CO_2$ differences is assessed using a two-sample Student's t-test at the 95% confidence level. Significance of differences is assessed relative to the interannual variability in the corresponding preindustrial control simulation.

### 2) Analysis Fields

In addition to the atmospheric variables examined in CP2019 (i.e., zonal mean wind, zonal mean temperature, surface temperature, 850 hPa zonal wind) we examine ocean variables relevant to understanding the evolution of the AMOC and its coupling to the atmosphere. In particular, in addition to examining the surface mixed layer depths we also examine sea surface temperatures, surface friction speed, horizontal ocean heat and salinity transports, as well as the net heat fluxes which, together with the net freshwater fluxes (F; inferred from precipitation minus evaporation (P-E)), provide information about the surface buoyancy forcing (Large and Yeager (2009)). In our simulations, the preindustrial climatological buoyancy forcing over the North Atlantic is dominated by the sum of the net heat fluxes ($Q = Q_H+Q_E+Q_S+Q_L$), which are defined to be positive into the ocean (Appendix Figure A1, left). These are further partitioned into their respective latent heat ($Q_E$) and sensible heat ($Q_H$) contributions, as we find that the net solar ($Q_S$) and longwave ($Q_L$) flux radiative contributions are negligible over the North Atlantic region (Appendix Figure A1, right).

Given our interest in the Northern Hemisphere and our expectations that stratospheric ozone feedbacks on the NH jet will occur during boreal winter (CP2019), we focus primarily on December-January-February (DJF). The ocean heat transport changes in our simulations are also most pronounced during DJF, consistent with the analyses presented in Romanou et al. (2023) and Orbe et al. (2023).

## 3. Results

### *a. Abrupt $2xCO_2$ and $4xCO_2$ Zonal Mean Wind Response: OMA versus NINT*

Before focusing on ozone feedbacks, we first review the OMA versus NINT differences in NH jet behavior that were presented in Zhang et al. (2023) (Figure 1). In the stratosphere the zonally averaged DJF wind response to 2- and $4xCO_2$ features an acceleration at nearly all latitudes, consistent with amplified warming in the tropical upper troposphere (Shaw (2019)) and increased cooling of the stratosphere with height (Garcia and Randel (2008)). Similar wind responses emerge in both the NINT and OMA configurations, except over northern high latitudes at $2xCO_2$, where the zonal winds in NINT weaken and the response is not statistically significant.

In the troposphere, however, there are noticeable differences between the OMA and NINT simulations. In particular, the NH midlatitude jet features a much stronger poleward shift in OMA, compared to NINT (Figures 3 and 6 in Zhang et al. (2023)). As discussed in that study, the stronger response in OMA results in enhanced eddy mixing along isentropes on the poleward flank of the NH jet, resulting in increased transport of tracers from the northern midlatitude surface to the Arctic (not shown). This difference between OMA and NINT occurs at both 2- and at $4xCO_2$, such that at $2xCO_2$ the NH jet response is opposite in sign between NINT and OMA, while at $4xCO_2$ the poleward jet shift is much stronger in OMA. In the SH, by comparison, the differences between OMA and NINT are much smaller and not statistically significant.

Zhang et al. (2023) hypothesized that the different behaviors of the NH jet between the NINT and OMA "total" responses were related to different responses in the behavior of the AMOC to increased $CO_2$ forcing (Figure 2). That is, despite an initial weakening, the AMOC eventually recovers to preindustrial values in the NINT $2xCO_2$ simulation, in contrast to the total response to $4xCO_2$ in which the AMOC is about 10 SV weaker than the preindustrial control (Fig. 2, left,

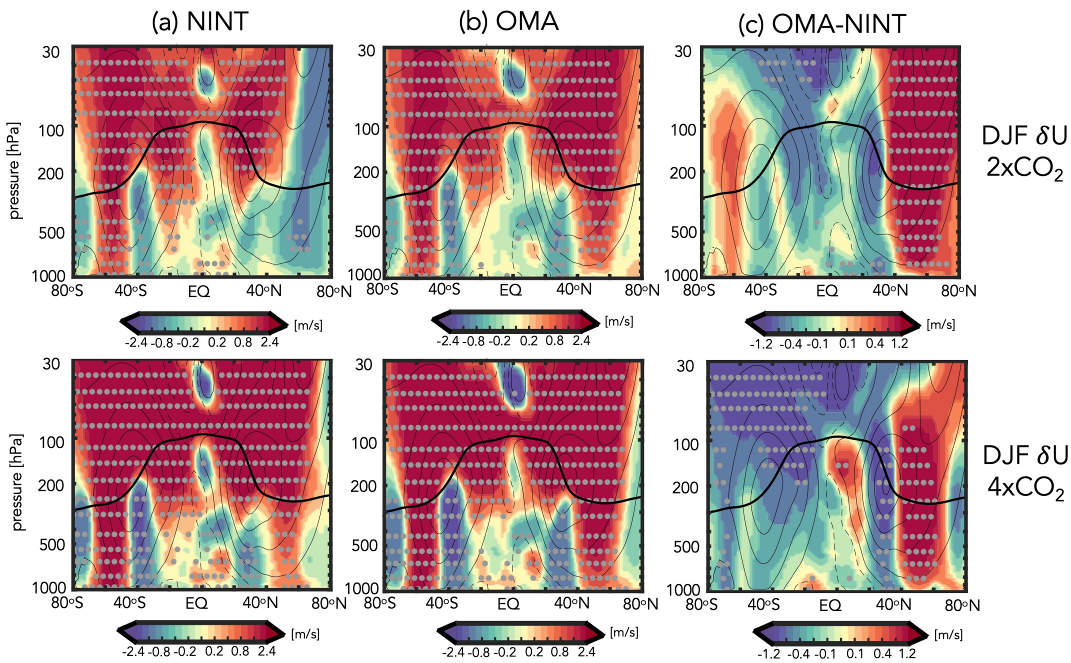


FIG. 1. Colors show the December-January-February (DJF) response of the zonal mean zonal winds, U, to an abrupt doubling (top) and quadrupling (bottom) of $CO_2$, averaged over years 100-150. Results are shown for NINT (a,d) and fully interactive OMA configurations (b,e), where one ensemble member has been used for each forcing scenario. The OMA - NINT differences are also shown (c,f). Black contours denote climatological mean preindustrial control DJF U values (contour interval: 8 m/s). Stippled regions are statistically significant and the black thick line shows the climatological mean tropopause in the preindustrial control NINT simulation. Note that all colorbar bounds are consistent with those used in Chiodo and Polvani (2019) in order to facilitate comparisons with that study.

black box). By comparison, in the OMA configuration, the AMOC weakens significantly more, by ~7 SV and ~17 SV in the 2- and $4xCO_2$ simulations, respectively (Fig. 2, right, black box).

As it is difficult to meaningfully interpret the zonal mean wind response in the NH, where there are large zonal variations in the midlatitude jet (Barnes and Polvani (2013); Simpson et al. (2014)), we next compare the 850 hPa zonal wind changes between the NINT and OMA $4xCO_2$ simulations, further distinguishing between "fast" and "total" responses (Figure 3). We begin with the NINT equilibrated or "total" response (i.e. years 100-150), which consists of a poleward jet shift over the Pacific basin and an acceleration and eastward extension of the jet over the Atlantic and Eurasia (Fig. 3b). This pattern is amplified in the OMA run (Fig. 3d), in which both the strengthening

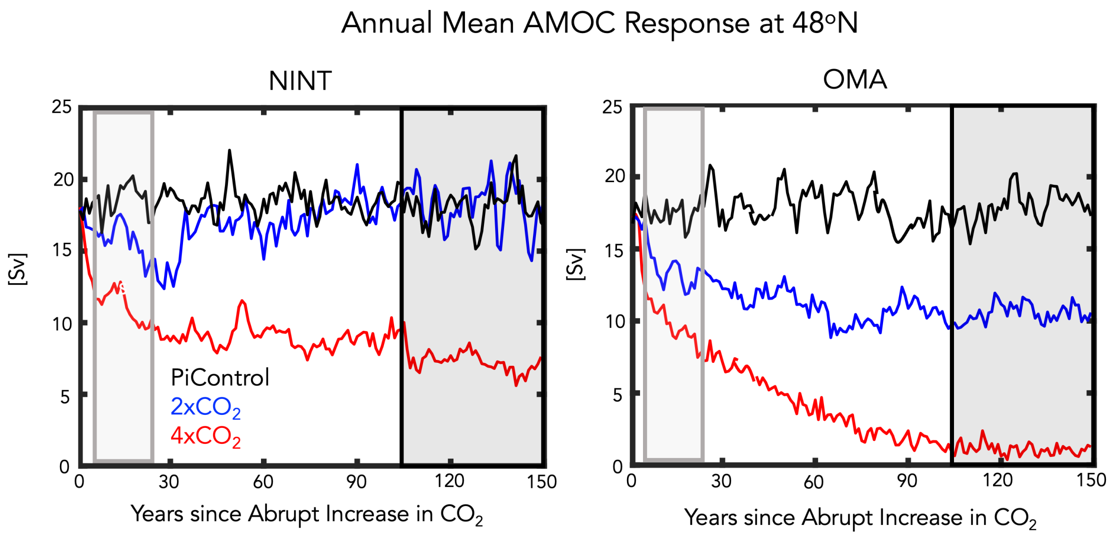


Fig. 2. Evolution of the annual mean maximum overturning stream function below 900 m in the Atlantic ocean, evaluated at 48°N, for the preindustrial control (black), abrupt 2x$CO_2$ (blue) and abrupt 4x$CO_2$ (red) simulations. Results for the NINT (left) and OMA (right) configurations are shown. Light grey and black shaded boxes denote the "fast" and "total" timescale response averaging periods.

and eastward extension of the jet over the Atlantic and its poleward shift over the Pacific are more pronounced. This amplified response in OMA over both the Pacific and Eurasia is also evident at 300 hPa (Appendix Figure A2b).

This wind response in OMA, relative to NINT, is consistent with the jet differences identified in Orbe et al. (2023) between two non-interactive simulations of the GISS low-top climate model in which only the AMOC strength differed. The enhanced and eastwardly extension of the North Atlantic jet is also consistent with previous studies employing water hosing simulations (e.g., Bellomo et al. (2023); Jackson et al. (2015)). This suggests that the jet differences between OMA and NINT on these longer timescales are primarily driven by differences in the AMOC response, as hypothesized in Zhang et al. (2023).

Figure 2 (grey boxes) highlights how the AMOC differences between OMA and NINT noted in Zhang et al. (2023) arise very early in the simulations (within the first 20 years). Over these years – which comprise the "fast" response – the impact of interactive chemistry on the zonal wind changes at 850 hPa is very different (Fig. 3a,c). In particular, over the Atlantic, interactive

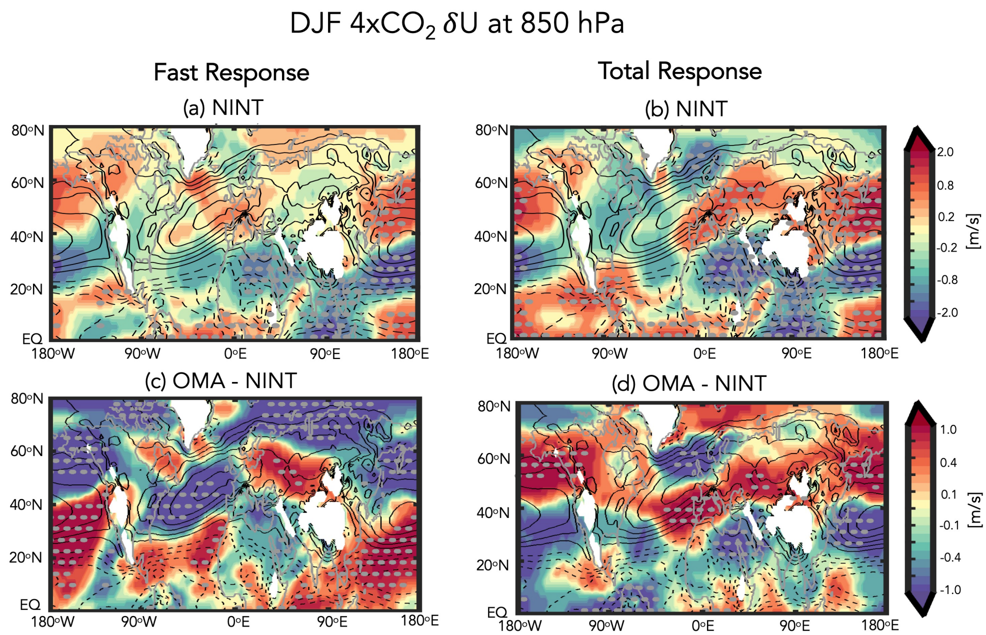


FIG. 3. Colors show the $4xCO_2$ (four member) ensemble mean change in the DJF 850 hPa zonal winds for the NINT configuration, decomposed into "fast" (i.e. years 5-20) (a) and "total" (i.e. years 100-150) (b) responses. The OMA - NINT fast and total differences are shown in (c) and (d), respectively. Note that one ensemble member is used in displaying the OMA - NINT differences (same as used in Figure 1). Black contours denote climatological mean preindustrial control DJF values (U contour interval: 2 m/s) and stippled regions are statistically significant.

composition results in a strong weakening over the midlatitude jet core and an acceleration on the equatorward flank of the jet (Fig. 3c). This wind change is also evident at 300 hPa (not examined in CP2019), where the winds accelerate on the equatorward and poleward flanks of the midlatitude and subtropical jets, respectively (Fig. A2a). Over the Pacific, where the midlatitude jet is more vertically coherent, interactive chemistry results in an anomalous equatorward jet shift relative to the NINT simulation at both 850 hPa (Fig. 3a) and 300 hPa (Fig. A2a).

This fast composition feedback that occurs over years 5-20 is consistent with the results from CP2019, who showed that the ozone response to $4xCO_2$ induces a weakening of the North Atlantic jet and a strengthening on its equatorward flank (see their Figure 6). This response is reminiscent of the negative phase of the NAO which previous studies have shown can result in a weaker AMOC (Delworth and Zeng (2016)). In CP2019, however, this response is realized through changes in stratospheric ozone alone, whereas in OMA all trace gases and aerosols are responding. Furthermore, the significance of this rapid response with only one ensemble member is uncertain, particularly during the first 5-20 years when the signal is confounded by large internal variability. To this end, next we present results from the larger (4-member) LINOZ ensemble to examine whether the fast response in the NH jet is related to stratospheric ozone changes.

*b. Abrupt 4x$CO_2$ Stratospheric Ozone and Temperature Responses: OMA versus LINOZ*

Before examining the circulation response in the LINOZ ensemble, we first compare the annually averaged ensemble mean LINOZ 4x$CO_2$ ozone response with that from the OMA simulation (Figure 4). The amplitude and pattern of the ozone response in the LINOZ ensemble (Fig. 4b) is generally very similar to the ozone response in the OMA simulation (Fig. 4a), consistent with Meraner et al. (2020), who showed that the response of ozone to a quadrupling of $CO_2$ is well captured using linearized ozone schemes. In both OMA and LINOZ configurations the pattern of the 4x$CO_2$ changes reflects a decrease in tropical LS ozone, associated with enhanced tropical upwelling (Garcia and Randel (2008)), and enhanced concentrations over high latitudes. Over all latitudes the ozone changes are statistically significant, relative to interannual variability in the preindustrial control simulation.

Over northern high latitudes there are some differences in the mid-to-lower stratosphere (~30-100 hPa) between LINOZ and OMA, generally consistent with Chiodo et al. (2018), who found that in this region the ozone response to $CO_2$ is more dependent on (nonlinear) chemical and transport feedbacks and thus more likely to be captured using a more comprehensive chemistry scheme. Furthermore, both simulations feature small changes in the troposphere. Overall, therefore, the LINOZ scheme captures the gross characteristics of the ozone abrupt 4x$CO_2$ response expected from previous studies. Note that most of this ozone response occurs in both simulations within the 5-20 years that comprise the "fast" response timescale, as shown in Chiodo et al. (2018) (see their Figure 7b), although full equilibration at high latitudes does take somewhat longer (not shown).

In response to the ozone changes to 4x$CO_2$ both the OMA simulation and LINOZ ensemble produce cooling in the tropical lower stratosphere and warming over high latitudes (Fig. 4c,d). The amplitude of the cooling is ~1.5-2K in the tropical lower stratosphere, and is more-or-less collocated with the region of largest ozone decreases. Further analysis of the temperature tendencies reveals

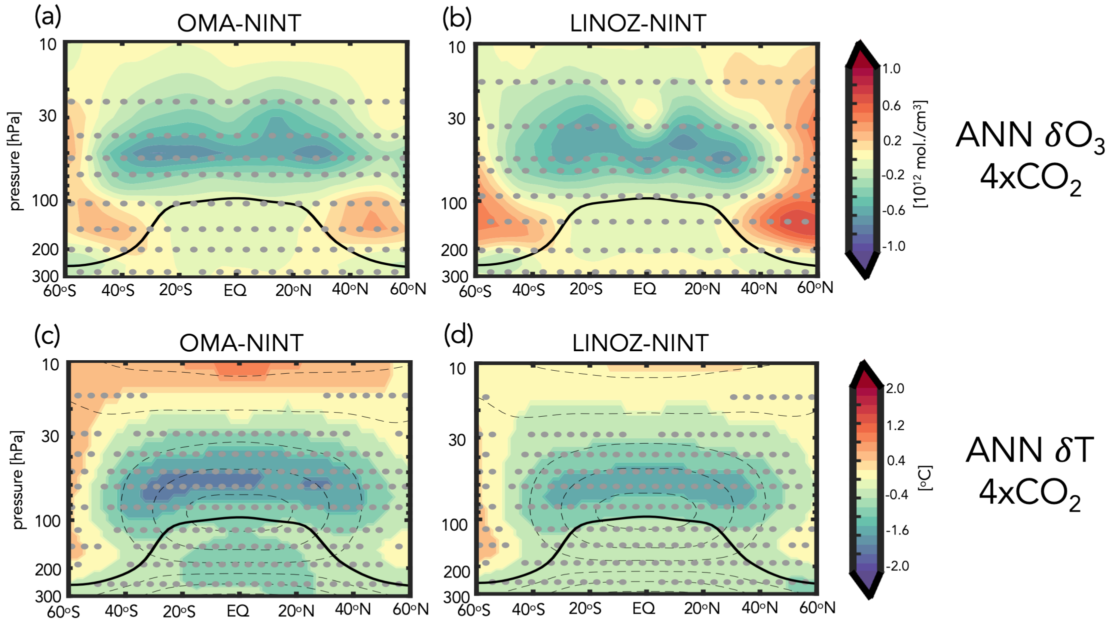


FIG. 4. Top: Colors show the annual averaged change in ozone number density in response to $4xCO_2$. Bottom: Colors show the annual averaged change in temperature in response to $4xCO_2$, relative to the $4xCO_2$ change in the NINT simulations. Results for OMA (left) and LINOZ (right) are shown in both rows and averaged over years 5-20. One simulation is shown for OMA and the four-member ensemble mean response is shown for LINOZ. Black dashed contours in the bottom panels show climatological mean preindustrial control temperatures (contour interval: 10 C). Stippled regions are statistically significant and the black thick line shows the climatological mean tropopause in the preindustrial control NINT simulation.

that in our model the cooler temperatures in the tropics and subtropics (40°S-40°N) are associated with reduced radiative heating, primarily in the shortwave component (not shown). Dynamically, comparisons of the $4xCO_2$ changes in the residual mean stream function show a weaker response in LINOZ, relative to NINT (not shown). This ozone feedback on the Brewer-Dobson circulation, first identified in DallaSanta et al. (2021a), contributes to reduced upwelling, adiabatic cooling, and ozone transport within the lower tropical stratosphere. These circulation changes are therefore not the primary drivers of the temperature response; rather, they are primarily determined by the shortwave radiative response to ozone changes (CP2019).

The temperature responses in both the OMA (Fig. 4c) and LINOZ (Fig. 4d) experiments are on the lower end of the 2-4K range documented in CP2019 as the differences shown reflect the 5-20 (not 100-150) year response (note that all colorbars used are consistent with that study to facilitate comparisons with their results). An important point to note is that the temperature changes due to ozone are of a similar magnitude to the temperature changes due to 4x$CO_2$ alone in the tropical lower stratosphere (i.e., considering no ozone feedback), where the stratosphere cools by ~2K in the NINT ensemble (not shown). The ozone changes present in LINOZ (and OMA) therefore represent a substantial (same order of magnitude) feedback on the $CO_2$-induced cooling in the stratosphere at this altitude.

### *c. Ozone Feedback on Northern Hemisphere Midlatitude Jet: Fast Response*

The temperature response due to ozone is dynamically consequential for the troposphere to the extent that it modifies temperature gradients (and winds) in the lower stratosphere. Indeed, the LINOZ ensemble shows a strong reduction of lower stratospheric temperature gradients in both hemispheres on both the fast and total response timescales (Fig. 5a,b). In the fast response, this reduction in the meridional temperature gradient near the tropopause has important consequences for the midlatitude jet in both hemispheres, particularly in the NH where it strengthens above and along the jet core and weakens on the poleward flank of the jet over latitudes north of ~ 50°N (Fig. 5c). The winds also accelerate equatorward of the jet core, relative to NINT, in both hemispheres, although the response is only statistically significant in our model in the NH. This ozone-induced response in the jet is very similar to the pattern of the wind response reported in CP2019 (see their Figures 4 and 5). As with the temperature changes occurring in the lower stratosphere, the wind response to ozone changes is similar in magnitude to the 4x$CO_2$ response (Fig. 1), again suggesting a substantial modulation of the circulation in both hemispheres by ozone changes alone.

In the lower troposphere (850 hPa) the fast response evident in the zonal mean zonal winds (Fig. 5c) is characterized by weakened winds north of 60°N over nearly all longitudes (Fig. 6a). By comparison, the weakened wind response south of 60°N is far more zonally asymmetric and concentrated over the Atlantic ocean, where negative wind anomalies are flanked equatorward by positive wind anomalies (Fig. 6a). Time series of the zonal winds over the North Atlantic at 850 hPa show evidence of this anomalous weakening of the jet in LINOZ occurring during the first 20 years (Fig. A3a), despite large internal variability. A similar response is also evident at 300 hPa (not shown), suggesting that the anomalous equatorward shift over the Atlantic during the fast

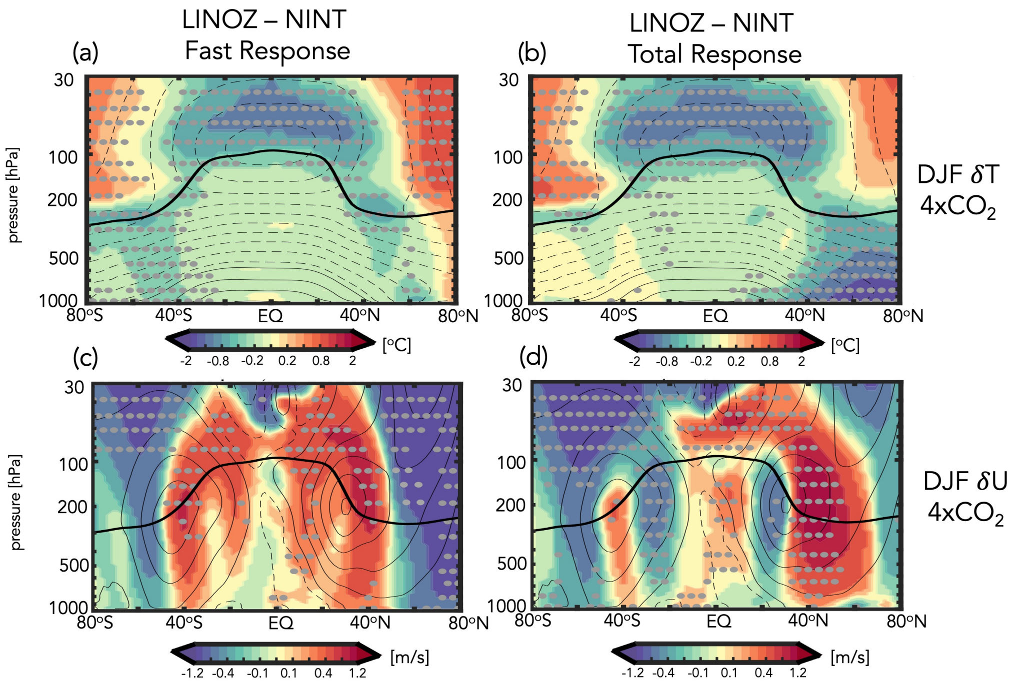


FIG. 5. Colors show the LINOZ-NINT ensemble mean difference in the DJF response of the zonal mean temperatures, T (top) and zonal winds, U (bottom) in response to an abrupt quadrupling of $CO_2$. Both LINOZ and NINT ensembles consist of four members. Responses are decomposed into "fast" (a,c) and "total" (b,d) changes. Contours denote climatological mean DJF values (T contour interval: 10 C; U contour interval: 8 m/s). Stippled regions are statistically significant and the black thick line shows the climatological mean tropopause in the preindustrial control simulation.

response comprises a barotropic response that extends from the upper troposphere down into the lower troposphere.

The LINOZ-NINT wind dipole at 850 hPa over the North Atlantic is very similar to the fast wind response captured in the fully interactive OMA simulation (Fig. 3c). This consistency with the response in OMA is also reflected at 300 hPa, where in both LINOZ and OMA configurations the winds accelerate between the climatological subtropical and midlatitude eddy-driven jets (Fig. A2a,c).

Over the Pacific, by comparison, the OMA and LINOZ responses are different, consistent with CP2019, who also found no robust ozone feedback over that basin (see their Figure 5). This lack of a robust ozone feedback over the Pacific is generally consistent with previous modeling and observational studies showing a much stronger signal of "downward" stratosphere-troposphere

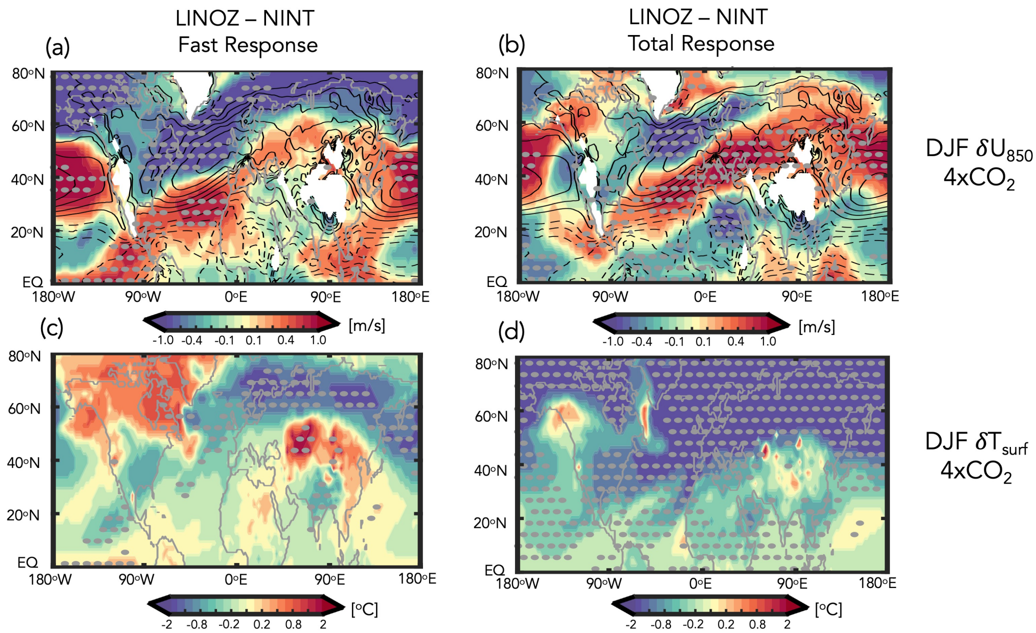


FIG. 6. Same as Figure 5, except showing the LINOZ-NINT DJF response in the 850 hPa zonal winds, $U_{850}$ (top) and surface temperatures, $T_{surf}$ (bottom). Contours in top panels denote climatological mean DJF values of $U_{850}$ (contour interval: 2 m/s). Note the similarity between the "fast" wind response shown in (a) and the CP2019 results (their Figure 6).

coupling over the Atlantic, relative to the Pacific (see Baldwin et al. (2021) and references therein), although this difference between sectors remains speculative and warrants closer inspection beyond the scope of the present study.

In addition to the near surface wind changes, the weakening of the North Atlantic jet in the LINOZ simulations is associated with warming over northern North America and cooling over the North Atlantic and over Eurasia, resembling the negative phase of the NAO (Fig. 6c). A similar surface temperature anomaly was identified in CP2019 (see their Figure 7) and in our model occur in conjunction with positive sea level pressure (SLP) anomalies over the Arctic (Appendix Figure A4, left), both features being reminiscent of a negative NAO.

*d. Ozone Feedback on Northern Hemisphere Midlatitude Jet: Total Response*

Interestingly, while the fast responses in the winds and temperatures in the LINOZ ensemble are highly consistent with the results from CP2019, our model also simulates a distinct "total" response characterized by strong cooling over the Arctic from the surface to the mid-to-upper troposphere (Fig. 5b). This cooling, which was not identified in CP2019, results in enhanced mid-to-lower tropospheric temperature gradients, prompting a strong acceleration of the winds at 50°N exceeding 2 m/s (Fig. 5d). Note that this acceleration at 50°N does not occur during the fast response, during which the winds weaken poleward of 50°N (Fig. 5c).

Zonally, the cooling over the Arctic occurring in the LINOZ ensemble during the total response primarily reflects hemispheric-wide cooling over the Arctic associated with an expansion of the North Atlantic Warming Hole (Fig. 6d, see also Zhang et al. (2023)). Thus, while both fast and total responses feature a similar weakening of the winds over the North Atlantic, this enhancement of meridional temperature gradients in the lower and mid troposphere drives an eastward extension and acceleration of the Atlantic jet over Europe and a poleward shift over the Pacific ocean during the total response (Fig. 6b). Time series of the zonal winds at 850 hPa show this strengthening of the midlatitude jet in LINOZ occurring on longer timescales (Fig. A3b), particularly over the Pacific and, to a lesser extent, over Europe. The jet acceleration over Europe is, by comparison, more pronounced in the upper troposphere (not shown) (Bellomo et al. 2021; Orbe et al. 2023).

By comparison, the eastward extension of the Atlantic jet is not evident during the fast response, nor is the poleward shift over the Pacific. This distinct behavior of the jet over the Pacific and Europe during the total response was also not captured in CP2019 and, as such, comprises a coupled ozone-ocean feedback that is distinct from what was reported in that study.

*e. Total Ozone Feedback: Modulation by the AMOC*

The "total" responses in the tropospheric winds and temperatures that occur in the LINOZ ensemble are not obviously linked to ozone-driven temperature changes in the stratosphere, which do not extend into the troposphere. What, then, is the driver of the lower tropospheric high latitude cooling, if it is not directly linked to ozone-driven stratospheric temperature changes?

As expected from the OMA and NINT results presented in Zhang et al. (2023) and summarized in Figure 2, we find that the strong cooling that occurs over the NH in the total LINOZ response is also related to a weakening of the AMOC at 4x$CO_2$ (Mitevski et al. (2021); Orbe et al. (2023)). In particular, Figure 7 shows stronger weakening of the AMOC in the LINOZ (green lines) ensemble, relative to NINT (blue lines) at both 26°N (left) and at 48°N (right). Despite large internal

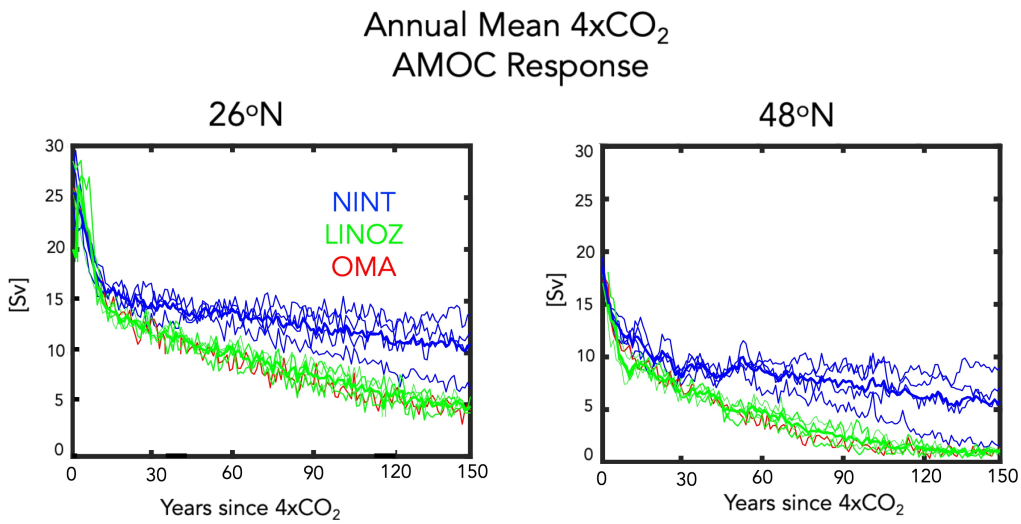


FIG. 7. Evolution of the annual mean maximum overturning stream function below 900 m in the Atlantic ocean, evaluated at 26°N (left) and 48°N (right) in response to $4xCO_2$. Results for the LINOZ and NINT ensembles are shown in green and blue, respectively (thick lines denote ensemble means). Red lines show the response in the OMA simulation.

variability, the LINOZ ensemble mean shows a more rapid decline of the AMOC, a difference that is evident at both latitudes. While the differences between the LINOZ and NINT ensemble means are most pronounced following year 20, a difference of ~2-3 SV is already established by year 20.

Interestingly, comparisons of the AMOC behavior in LINOZ with the fully interactive OMA simulation (red line) shows a striking similarity (and the mechanism of these changes is also similar, as shown in Section 3f). This similarity is surprising, given that other (non-ozone) trace gases and aerosols are also evolving in the OMA experiment. In particular, Rind et al. (2018), using a previous version of the model, observed an indirect effect of natural aerosols (primarily sea salt) on AMOC stability. They showed that aerosols enhanced the local cooling of SSTs in regions of increased cloud cover in a warmer climate by acting as condensation nuclei and thereby raising cloud optical thickness and ocean surface cooling. This surface cooling was then linked to reduced evaporation relative to precipitation, resulting in anomalously positive surface freshwater forcing and reduced North Atlantic Deep Water (NADW) production. That study, however, focused on aerosol-induced AMOC cessations occurring on multicentennial timescales long after the initial (abrupt) warming. By comparison, the results in Figure 7 identify an impact of ozone on the ensemble mean AMOC responses that occurs within the first 20 years of the initial $CO_2$ forcing – that is, over the period during which ozone is also rapidly evolving (Chiodo et al. 2018) and stratospheric temperature gradients are most impacted by changes in ozone (not aerosols). Our results, therefore, highlight that during this time frame the AMOC can be as (if not more) sensitive to wind-driven buoyancy changes forced by stratospheric ozone anomalies as they are to aerosol-induced changes in freshwater forcing.

Before elucidating the mechanism of the AMOC changes in the LINOZ ensemble, we first identify the region over which the largest differences in mixed layer depth begin to emerge between the LINOZ (OMA) and NINT simulations. In particular, the weaker AMOC in the LINOZ and OMA runs is found to be accompanied by a rapid reduction in mixed layer depths, which occur primarily in the Irminger Sea region (55°N-65°N, 40°W-20°W) (Figure 8). Over that region, an ensemble mean LINOZ vs. NINT difference of ~200 m is established by year ~20. The mixed layer depth differences among the configurations in the Labrador Sea are, by comparison, negligible. East of the Irminger Sea (i.e., 55°N-65°N, 20°W-0°) we also identify differences between the ensembles (not shown), but these emerge later, suggesting that the Irminger Sea changes are likely the initiators of the differences in AMOC behavior between the NINT and LINOZ ensembles. The same region was identified in Romanou et al. (2023) as being key for determining the sensitivity of the AMOC in various SSP 2-4.5 ensemble runs, albeit for simulations conducted using the lower vertical resolution GISS climate model.

### *f. Ozone Feedback Dependence on the AMOC: Linking Fast and Total Responses*

Is the fact that the AMOC declines more rapidly in the LINOZ ensemble – and the OMA simulation – a response to the ozone changes in those simulations or just a coincidence? In the fast response the zonal wind changes over the North Atlantic reflect a weakening of the jet core that is flanked equatorward by positive anomalies, resembling a negative NAO pattern. Indeed, a negative (positive) NAO has been associated with a weaker (stronger) AMOC in idealized climate model experiments in which heat is artificially added (extracted) to/from the subpolar gyre, resulting in reduced (increased) NADW formation (Delworth and Zeng (2016)). Here we argue that such a

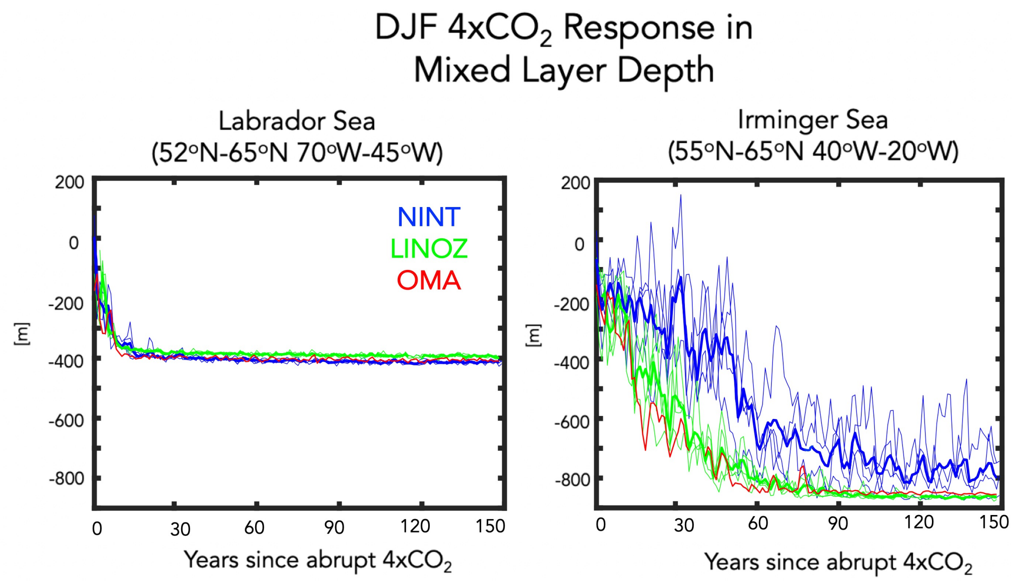


FIG. 8. Changes in the DJF mixed layer depths, evaluated over the Labrador Sea (left) and Irminger Sea (right) in response to 4x$CO_2$, relative to the preindustrial control simulations. Results for the LINOZ and NINT ensembles are shown in green and blue, respectively (thick lines denote ensemble means). Red lines show the response in the OMA simulation.

mechanism is present in our model simulations, resulting in a long-term modulation of the NH midlatitude jet by ozone that occurs indirectly through changes in the AMOC.

In particular, Figure 9 shows maps of the surface zonal wind, surface friction speed, mixed layer depth, net heat fluxes, sea surface temperatures, and north-south heat and salinity ocean transports, averaged over years 1-5 (averages over years 5-20 are shown in Figure 10). In response to an abrupt quadrupling of $CO_2$, the surface winds weaken over the subpolar North Atlantic region in NINT, leading to a weak acceleration of the zonal winds on the poleward flank of the North Atlantic jet (~60°N-70°N) (Fig. 9a, top). Over the subpolar North Atlantic the weakening of the surface winds leads to a significant reduction in surface friction speed (Fig. 9b, top). At the same time, there is a reduction in mixed layer depths (Fig. 9c, top), as well as increased heat flux into the ocean (in the form of reduced latent heat fluxes out of the ocean) (Fig. 9d, top) and warmer sea surface temperatures (Fig. 9e, top). The reduced surface density during the first 20 years associated with these warmer temperatures lead to a rapid decrease in mixed layer depth by some 200 m (Figure

8) and the overturning circulation by ~ 40% (Figure 7) in NINT. At these early years the changes in meridional heat and salinity transports over the Irminger Sea are relatively small (Fig. 9fg, top).

However, in response to the ozone changes captured in the LINOZ ensemble during years 1-5, there is an even stronger reduction in the surface zonal winds and friction speed (Fig. 9 ab, bottom), consistent with the negative NAO response evident in the 850 hPa zonal winds (Fig. 6a). The surface friction changes align closely with the reduced mixed layer depths which extend well into the Irminger Sea region and over latitudes further south of the subpolar gyre (Fig. 9c, bottom).

The reductions in mixed layer depth that occur over the Irminger Sea are likely driven by the reductions in surface wind speed which increase (primarily latent) heat fluxes into the ocean (Fig. 9d, bottom), driving warmer sea surface temperatures in LINOZ, relative to NINT (Fig. 9e, bottom). The sign of the response of the heat fluxes in the subpolar gyre region is consistent with previous studies showing that a positive (negative) phase of the NAO implies reduced (enhanced) atmosphere to ocean heat fluxes (Delworth et al. (2017)). Furthermore, the spatial pattern of the heat flux response is very similar to the NAO heat flux composites that were prescribed in Delworth and Zeng (2016) and inferred from observations in Ma et al. (2020) (see their Figure 6), who showed that there is much greater heat loss from the ocean over the subpolar region in association with a jet strengthening.

At the same time, the changes in freshwater forcing (P-E) during this time period are negligible such that the net buoyancy forcing comprising the sum of both net heat and freshwater fluxes (~Q+F) is positive. This stabilizing buoyancy forcing from surface warming makes the mixed layer depths shallower by suppressing convective mixing, shutting down NADW production (Alexander et al. (2000); Kantha and Clayson (2000)). There is also an initial change in the north-south heat and salt transports that is collocated with the dipole anomaly in the surface friction speed, promoting anomalous poleward salt and heat transport into the subpolar gyre (Fig. 9fg, bottom). This feature is confined to the top few ocean layers (not shown) and the implied anomalous heat transport could be contributing to the warmer sea surface temperatures in that region, in addition to the surface heat flux changes. Note that the emergence of these surface changes happens somewhat earlier than the response in the AMOC, which shows clearer differences by year ~10 (Fig. 7). While a thorough examination of potential lags in the response of the AMOC, relative to the surface, are beyond the scope of this study, this will be examined in future work.

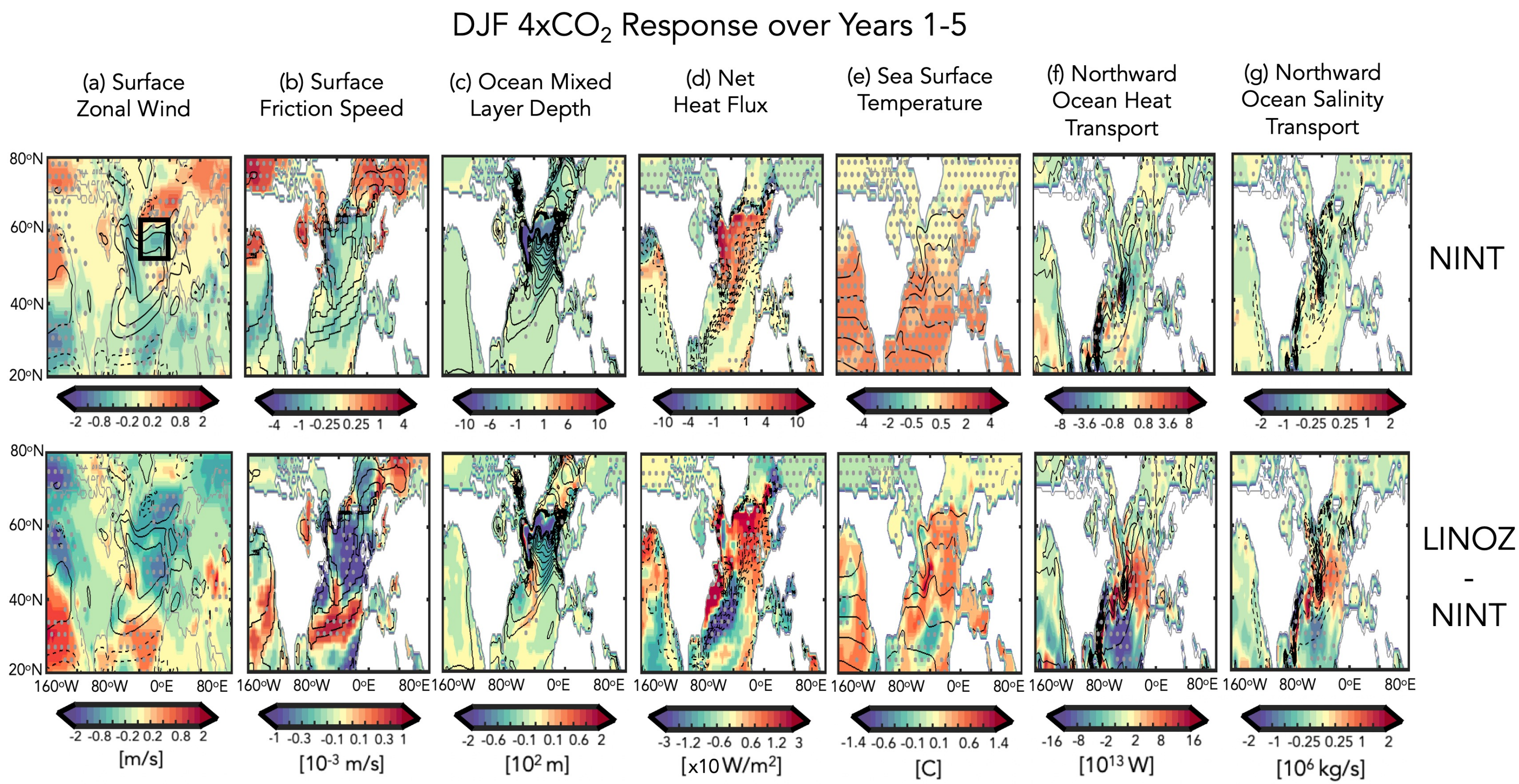


FIG. 9. Top panels: Colors show the December-January-February (DJF) response of the surface zonal wind (a), surface friction speed (b), ocean mixed layer depth (c), net heat flux (sum of sensible plus latent heat) (d), sea surface temperature (e) and northward heat (f) and salt (g) transports in response to an abrupt quadrupling of $CO_2$. Results are shown for the 4-member ensemble averaged NINT configuration. Bottom panels: Same as top panels, except showing the LINOZ minus NINT ensemble mean difference. For both top and bottom panels, responses have been averaged over years 1-5 since "branching" from the preindustrial control simulation. Stippled regions are statistically significant and black contours denote climatological mean preindustrial control DJF values. Contour intervals: surface zonal wind [2 m/s], surface friction speed [$2.5\text{x}10^{-3}$ m/s], mixed layer depth [60 m], net heat flux [30 W/m$^2$], sea surface temperature interval [2°C], northward heat flux [$2\text{x}10^{12}$ W], and northward salt flux [$10^6$ kg/s]. The black box in (a) bounds the Irminger Sea region over which the spatial averages in Figure 8b and Figure 11 are evaluated.

Over the ensuing years (5-20) a similar pattern is maintained in the LINOZ ensemble (Figure 10, middle row). The reduction in NADW, however, results in reduced northward heat and salinity transports (Fig. 10 fg, middle) throughout the ocean columm. While this results in cooler SSTs south of the subpolar gyre region (Fig. 10e, middle), which otherwise might enhance the density of the near-surface water masses, the reduced northward salinity transports prevent the AMOC from restarting. Interestingly, the results from the OMA simulation show a very similar response as the LINOZ ensemble (Figure 10, bottom row), suggesting that stratospheric ozone changes in that simulation are also likely the primary driver of the weaker AMOC in that model configuration. This sequence of processes linking the surface wind changes to anomalous heat fluxes and reduced NADW is basically identical to what is outlined in Figure 4 of Delworth and Zeng (2016) and Figure 1 of Khatri et al. (2022). Additional analysis of the 2x$CO_2$ simulations, which feature a stronger AMOC decline in OMA (and LINOZ) compared to NINT (Figure 2), reveals that a similar mechanism for reduced NADW production occurs at lower $CO_2$ forcing (not shown).

Examining the timescale of the responses of the variables shown in Figures 9 and 10 reinforces the strong coupling between the changes in surface friction speed, sea surface temperature, latent heat fluxes and mixed layer depth changes over the Irminger Sea region (Figure 11a-d). Despite large internal variability, there is a clear separation between the LINOZ (and OMA) and NINT ensembles that emerges ~ year 15 (black dashed lines). The changes in sensible heat emerge after the latent heat fluxes (Fig. 11e), suggesting that the latter play a more important role in initializing the heat flux differences in LINOZ (and OMA), relative to NINT.

Finally, while they may contribute to enhanced positive buoyancy forcing later in the integrations, the freshwater forcing anomalies (F = P-E) are shown to be negligible during the initial years following the abrupt quadrupling of $CO_2$ (Fig. 11f), indicating that the primary driver of the initial difference between the LINOZ (and OMA) and NINT runs is related to the surface wind-driven changes as they impact the latent heat fluxes into the ocean. This is consistent with Roach et al. (2022) who showed a much stronger correlation between AMOC strength at 26°N and the heat component of the surface buoyancy flux, relative to the freshwater component, in various experiments using the Community Earth System Model version 1 (CESM1) in which the winds over the subpolar gyre were nudged to reanalysis values. Note that in our model other potential contributors to freshwater forcing from sea ice do reveal differences between the LINOZ, OMA

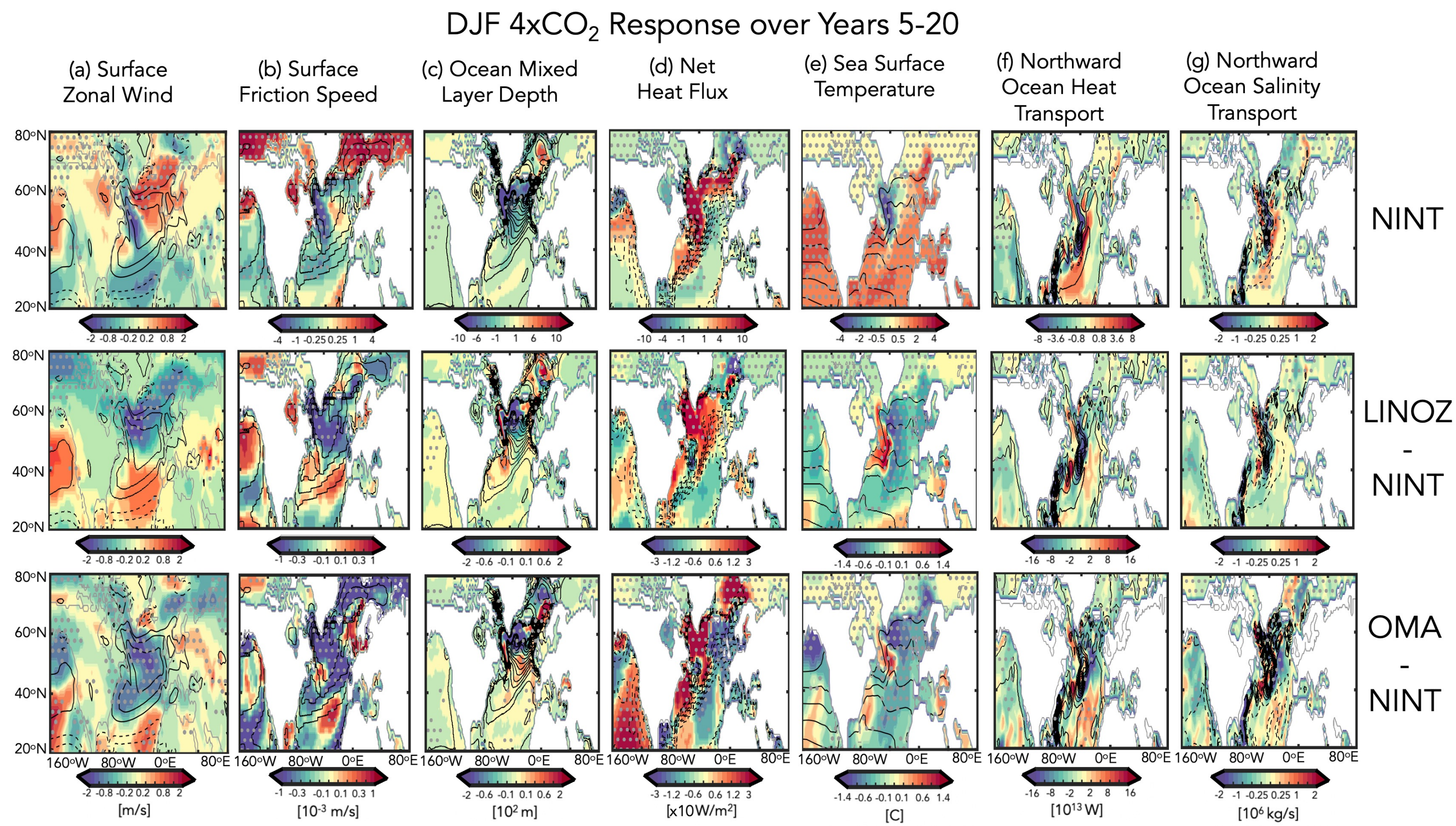


FIG. 10. Same as Figure 9, except showing the responses, averaged over years 5-20. An extra row at the bottom has been added, showing the OMA - NINT differences, where the ensemble members shown in Figures 1, 2 and 3 have been used. Same contour intervals and colorbars have been used as in Fig. 9.

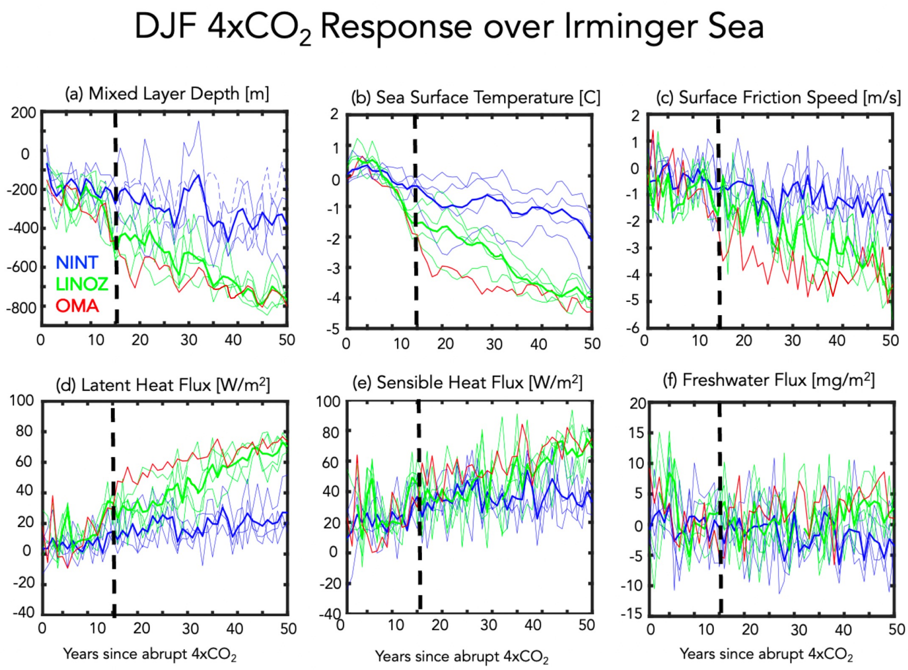


FIG. 11. Changes in the DJF mixed layer depths (a), sea surface temperatures (b), surface friction speed (c), latent heat fluxes (d), sensible heat fluxes (e) and precipitation minus evaporation (f) in response to 4xCO$_2$, relative to the preindustrial control simulations. Averages are performed over the Irminger Sea (55°N-65°N, 40°W-20°W) and the x-axis is restricted to years 1-50 in order to highlight the fast timescales on which the mixed layer depths, surface friction speed and heat fluxes evolve together. Results for the LINOZ and NINT ensembles are shown in green and blue, respectively (thick lines denote ensemble means). Red lines show the response in the OMA simulation. Black vertical lines indicate ~15 at which point the mixed layer depth responses in the LINOZ and NINT ensembles diverge. Note that the freshwater flux unit of 1 mg/m$^2$ per second (≡ 0.0864 mm/day ≡ 3.1 cm/year) is used, because at 5°C it contributes approximately the same ocean density flux as the heat flux unit of 1 W/m$^2$ (Large and Yeager (2009)).

and NINT ensembles, but these emerge several years (i.e., years ~20-30) after the changes in sea surface temperatures and heat fluxes (not shown).

### *g. Ozone Driver of AMOC Changes: Fixed SST and SIC Results*

So far, we have shown that the stratospheric ozone changes that occur in response to 4xCO$_2$ result in a negative NAO response over the North Atlantic (Fig. 5,6). In our model this triggers a more rapid decline of the AMOC (Fig. 7) through surface-wind driven changes in heat fluxes into the ocean (Fig. 9,10). While the time series analysis (Fig. 11) reveals that the AMOC changes in the LINOZ (OMA) ensemble occur on similar timescales as the wind (and heat flux) changes, one potentially confounding factor is the fact that the AMOC reduction itself results in reduced wind speeds over the subpolar gyre region. These reduced near-surface winds are associated with an anomalous anticyclonic flow pattern (Fig. A4, left; also discussed in Gervais et al. (2019); Romanou et al. (2023); Orbe et al. (2023)), which could contribute to the reduced heat fluxes and subsequent changes in NADW production. Therefore, to more convincingly link the surface wind speed changes to the stratospheric ozone changes aloft, we next examine results from the fixed preindustrial control SST and SIC experiments.

Figure 12 shows the ozone-induced zonal wind and temperature changes averaged over the last twenty years of the fixed preindustrial control SST and SIC experiments in which the time-varying zonally varying ozone from the 4x$CO_2$ LINOZ ensemble is prescribed (Fig. 12 a,b). Recall that in the fixed SST and SIC experiments, only the ozone evolution differs from the preindustrial control simulation, as $CO_2$, SSTs and SIC are all set to preindustrial values. Comparisons with results from the fully coupled LINOZ "fast" response (see Fig. 5a,c) reveal a very similar picture. This similarity between the fully coupled fast response and the fixed preindustrial control SST and SIC experiments is striking, both featuring a similar change in the NH jet associated with reduced temperature gradients in the lower stratosphere as first reported in CP2019.

Comparisons of the 850 hPa zonal winds and surface temperatures over the North Atlantic (Fig. 12c,d) also reveal a strikingly similar response between the fully coupled ensemble and the fixed preindustrial control SST and SIC experiments (compare with Fig. 6a,c). Over the Atlantic this similarity also holds in the sea level pressure response (Fig. A4, right). The consistency in the sea level pressure changes is interesting as it suggests that over the North Atlantic stratospheric ozone changes alone can result in a significant reduction in the near surface winds that is on the same order (if not larger than) the 4x$CO_2$ response. In our coupled atmosphere-ocean model this additionally results in heat flux changes that are large enough to reduce NADW production, resulting in a significant (i.e. ~30-40%) long-term change in AMOC strength.

Finally, though not reported in depth here, we have performed an additional four-member ensemble that is identical to the fixed SST and SIC runs, with respect to external forcings (i.e., preindustrial background $CO_2$, LINOZ 4x$CO_2$ $O_3$), except run using the coupled atmosphere-ocean model. Preliminary analysis of the "fast response" (5-20 years) in these experiments (not shown) reveals very consistent ozone feedbacks on stratospheric temperatures, zonal mean winds and 850 hPa zonal winds, compared to those captured in the coupled LINOZ 4x$CO_2$ simulations. Over longer timescales (> 30 years), however, the response of the coupled ocean-atmosphere system is more muted in the absence of any background 4x$CO_2$ forcing, especially the responses in surface winds, net heat fluxes into the ocean and mixed layer depths. This result is perhaps not surprising, given that the reduced surface zonal winds and mixed layer depths over the subpolar gyre were identified as responses to an AMOC weakening in the ocean model employed in this study (Orbe et al. 2023). This suggests that the AMOC response to stratospheric ozone feedbacks depends sensitively on the background $CO_2$ forcing, although a systematic examination of this dependence is beyond the scope of the current manuscript and will be explored in future work.

## 4. Conclusions

Here we have used the NASA GISS coupled atmosphere-ocean high-top model (E2.2-G) to examine how coupled changes in stratospheric ozone and the ocean circulation both influence the abrupt 4x$CO_2$ response of the NH midlatitude jet. Our key results are as follows:

- The NH midlatitude jet response to 4x$CO_2$ is modulated by coupled feedbacks from both stratospheric ozone and the AMOC, which occur on "fast" (5-20 year) and "total" (100-150 year) timescales, respectively.
- In the "fast" response, the zonal mean jet weakens (strengthens) on its poleward (equatorward) flank, consistent with reduced LS temperature gradients associated with ozone loss in the tropics. This response is zonally asymmetric and is expressed as a negative NAO-like pattern, consisting of weaker zonal surface winds over the North Atlantic, as reported in CP2019.
- The weaker winds over the North Atlantic occurring during the "fast" response are associated with increased (primarily latent) heat fluxes into the ocean, which initially result in warmer SSTs over the subpolar gyre region, reducing NADW production and leading to more rapid weakening of the AMOC.
- A reduced AMOC leads to widespread cooling over the Arctic which enhance mid-to-lower tropospheric temperature gradients, resulting in an eastward acceleration of the Atlantic jet and

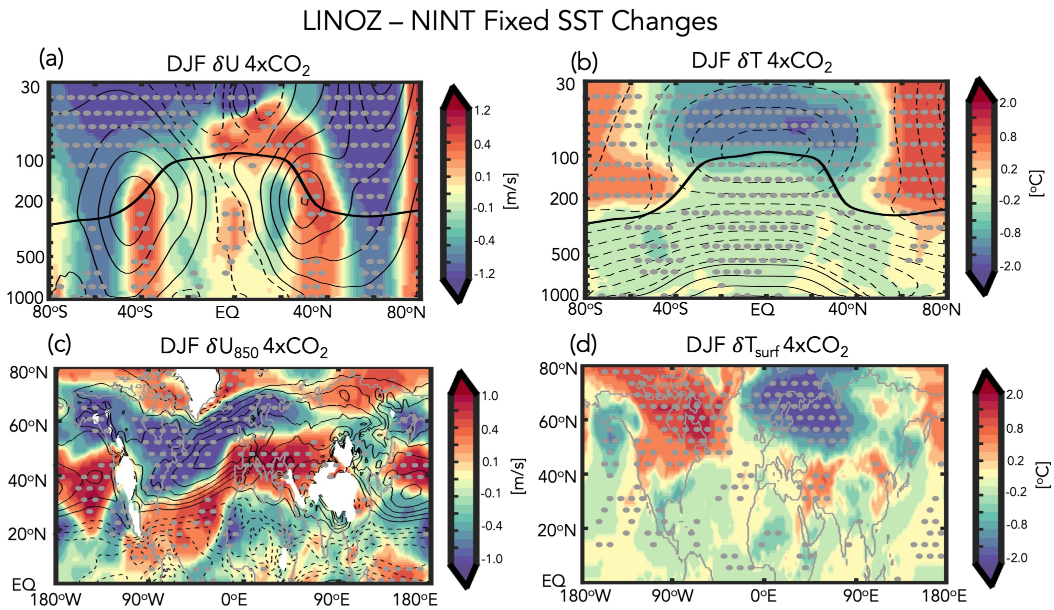


FIG. 12. Top panels: Colors show the $4xCO_2$ ensemble mean response in zonal mean zonal winds, U (a), temperatures, T (b), 850 hPa zonal winds, $U_{850}$ (c) and surface temperature, $T_{surf}$ (d) in the prescribed SST and SIC experiments in which the time-evolving $4xCO_2$ ensemble mean LINOZ ozone response is prescribed. Note that SSTs, SICs and background $CO_2$ are all set to preindustrial values. Averages are shown over the last 20 years (years 40-60) of the integrations. Black contours, where shown, denote climatological mean preindustrial control DJF values (U contour interval: 8 m/s; T contour interval: 10 C; $U_{850}$ contour interval: 2 m/s). Stippled regions are statistically significant and the black thick line in the top panels shows the climatological mean tropopause in the preindustrial control simulation.

a poleward shift of the Pacific jet. The regional pattern of this "total" response is consistent with previously reported impacts of a weakened AMOC on the NH midlatitude jet (e.g., Bellomo et al. (2021); Liu et al. (2020); Orbe et al. (2023); Zhang et al. (2023)).

Taken together, the findings listed above indicate that the stratospheric ozone feedback on the NH midlatitude jet reported in CP2019 is coupled to the behavior of the AMOC during the "fast" response, wherein the jet weakens over the North Atlantic. In our model, this wind response extends to the surface, resulting in reduced heat fluxes out of the subpolar gyre region and a more rapid decline of the AMOC. On longer timescales, these changes in the AMOC subsequently drive a poleward shift in the NH midlatitude jet. Unlike the "fast" response, this "total" timescale response in the NH jet to changes in stratospheric ozone has not been previously reported, to the best of our knowledge. This may reflect differing sensitivities of the AMOC among models and our results will, of course, need to be tested using other models to assess robustness.

Another intriguing result from this study is that the stronger decline of the AMOC in the LINOZ ensemble does not appear to be a coincidence. Rather, in our model, the "fast" ozone and "total" AMOC feedbacks on the NH jet are coupled through surface-wind driven changes in heat fluxes into the ocean. Key here is the fact that this sensitivity in the AMOC is driven only by changes in stratospheric ozone, which we have isolated from changes in other trace gases and aerosols.

This last point is important to note, as previous studies have long shown that interactive atmospheric composition can strongly influence the AMOC, but place an almost exclusive focus on the role of aerosols (Booth et al. (2012); Cowan and Cai (2013); Swingedouw et al. (2015); Zhang et al. (2013, 2019); Robson et al. (2022)). In particular, Rind et al. (2018) identified a larger sensitivity of the AMOC response to global warming using an interactive configuration of the CMIP5 version of the GISS climate model (GISS-E2-R), compared to a non-interactive version. In that study, multicentennial cessations of the AMOC were found to occur in simulations in which natural aerosols (primarily sea salt) were allowed to locally cool sea surface temperatures through their influence on cloud optical thickness; these cooler SSTs were then linked to reduced evaporation relative to precipitation, resulting in positive surface freshwater forcing and reduced NADW production. Unlike in that study, the mechanism proposed here only invokes changes in stratospheric ozone, not aerosols, and to the best of our knowledge, no study has previously demonstrated an impact of stratospheric ozone changes alone on the AMOC response to a quadrupling of $CO_2$. Despite the different mechanisms at play, however, our results are generally consistent with those from Rind et al. (2018) in that they highlight the need for renewed focus on surface flux observations to help assess overturning stability.

An important caveat with our results is related to known biases in vertical mixing and NADW production in the ocean component of the GISS model (Miller et al. (2021); Romanou et al. (2023)) which likely explain why the low-top version of the coupled atmosphere-ocean climate model (E2.1-G) exhibits a more sensitive AMOC response to a quadrupling of $CO_2$, compared to some other models (Bellomo et al. (2021)). An important point to highlight, however, is that the high-top model employed in this study is much less sensitive, as the AMOC weakens by $\sim$10

SV in response to $4xCO_2$, compared to a complete collapse in E2.1-G (see Figure 31 in Rind et al. (2020)). That study showed that this may be related to differences in the parameterization of rainfall evaporation associated with moist convective precipitation, which they show has a strong influence on the AMOC sensitivity in the GISS model via its effect on moisture loading in the atmosphere. While an exhaustive comparison between the models is beyond the scope of this study, the relevant point here is that the $4xCO_2$ AMOC response simulated in the E2.2-G NINT ensemble is well within the CMIP5 and CMIP6 ranges documented in Mitevski et al. (2021) (see their Supplementary Figure S3).

An important next step for future research is to identify the forcings under which this influence from stratospheric ozone is evident. Our preliminary analysis of the coupled atmosphere-ocean response to $4xCO_2$ stratospheric ozone changes reveals a much more muted ocean response in experiments where the background $CO_2$ forcing is fixed to preindustrial values, compared to simulations in which $CO_2$ increases. This suggests that the ozone feedback on the AMOC depends on the background $CO_2$ forcing and may hinge on the model's so-called "hysteresis" or threshold beyond which the AMOC continues to weaken, even upon reversal of the forcing. Indeed, recent studies (Romanou et al. 2023; Orbe et al. 2023) have identified hysteresis not only in the ocean model employed in this study, but also in the much broader CMIP6 model archive (Jackson et al. 2022). This hypothesis, however, remains highly speculative and future work will focus on exploring the $CO_2$ forcing-dependence of the ozone feedback and its relationship with hysteresis.

Another related issue concerns the need to examine whether the ozone feedback occurs in more comprehensive scenarios using transient forcing. Although not examined in equal depth, results from the more realistic $1\%CO_2$ transient simulations also show a greater weakening of the AMOC in OMA, relative to NINT, indicating that the findings presented here are not an artifact of the abruptness of the forcing (not shown). Analysis of the more comprehensive historical and future Shared Socioeconomic Pathway (SSP) (Meinshausen et al. (2020)) integrations is currently underway to identify other factors, including aerosols and the solar cycle (Muthers et al. (2016)), which are likely to influence the ocean circulation. For sake of brevity, however, we reserve further discussion of the more comprehensive results for future work.

Finally, our results linking the fast timescale jet response to the ensuing AMOC changes underscore the profound impact that changes in lower stratospheric winds alone can have on surface climate, as highlighted in Sigmond and Scinocca (2010). Quite remarkably, our fixed SST and SIC experiments showed that these lower stratospheric wind changes are driven primarily by changes in ozone and not by background changes in $CO_2$ or in sea surface boundary conditions. Taken together, our results suggest that more attention needs to be paid to understanding the time-evolving response of the coupled Earth system to future ozone changes, with a focus on changes in ocean heat transport and how these feed back on the NH jet stream.

*Acknowledgments.* C.O. acknowledges helpful discussions with Lettie Roach, Ivan Mitevski and Lorenzo Polvani. G.C. acknowledges support by the SNSF with the "Ambizione" grant N. PZ00P2_180043. Climate modeling at GISS is supported by the NASA Modeling, Analysis and Prediction program, and resources supporting this work were provided by the NASA High-End Computing (HEC) Program through the NASA Center for Climate Simulation (NCCS) at Goddard Space Flight Center.

*Data availability statement.* The NINT and OMA GISS E2.2-G simulations used in the study are available at the CMIP6 archive via the Earth System Grid Federation (`https://esgf-node.llnl.gov/`), where NINT and OMA are respectively denoted as "physics version 1" and "physics version 3". The specific simulations used here are the PiControl, abrupt-2x$CO_2$, and abrupt-4x$CO_2$ r1i1p1f1 (NINT) and r1i1p3f1 (OMA) runs. Output needed to reproduce all figures showing the additional three NINT 4x$CO_2$ simulations, fixed SST simulations as well the four-member LINOZ ensemble is available online at `https://gmao.gsfc.nasa.gov/gmaoftp/corbe/AMOC_Linoz/Data/`. All GISS ModelE components are open source and available at http://www.giss.nasa.gov/tools/modelE/.

# APPENDIX

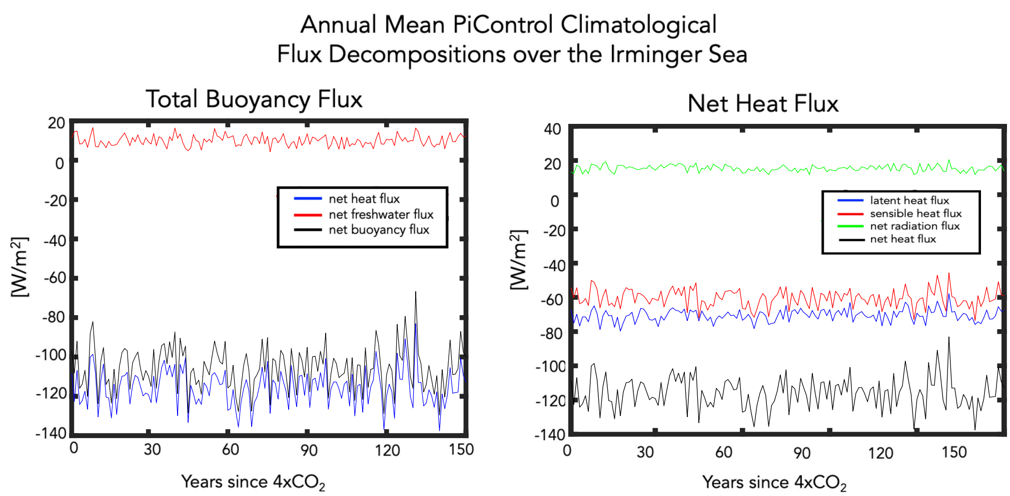


FIG. A1. Left: Decomposition of the net surface buoyancy flux (black) into contributions from net heat (blue) and net freshwater (red) fluxes. Right: Further decomposition of the net surface heat flux (black) into contributions from latent heat fluxes ($Q_E$ (blue)), sensible heat fluxes ($Q_H$ (red)), and combined solar and longwave radiative fluxes ($Q_S$+$Q_L$ (green)). Results are shown for 150 years of the NINT preindustrial control (PiControl) simulation, evaluated over the Irminger Sea.

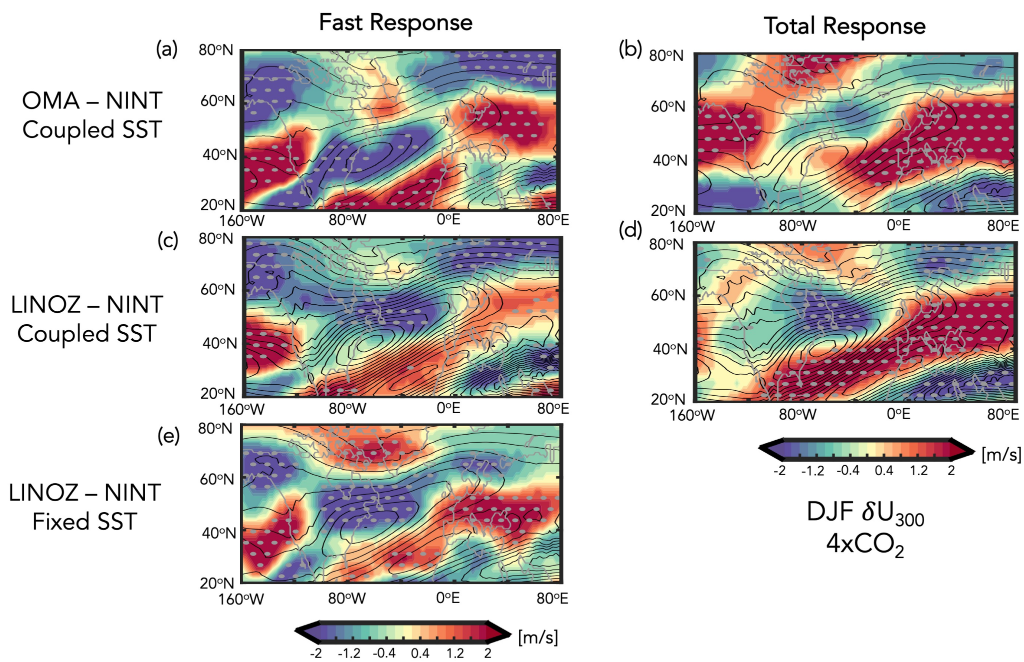


FIG. A2. Colors show the coupled atmosphere-ocean OMA - NINT (a,b) and LINOZ - NINT (c,d) $4xCO_2$ changes in the DJF 300 hPa zonal winds. One ensemble member is used in the top panels, compared to four members in the middle row. Panel e shows results from the atmosphere-only ensemble in which the time-evolving $4xCO_2$ ensemble mean LINOZ ozone response is prescribed and the SSTs, SICs, and background $CO_2$ are set to preindustrial values. Left and right panels in the top and middle rows show the responses decomposed into "fast" (i.e. years 5-20) (a,c) and "total" (i.e. years 100-150) (b,d) responses. Averages over years 40-60 are shown for the prescribed SST and SIC experiments in panel e, which equilibrate much more rapidly, compared to the coupled experiments. Black contours denote climatological mean preindustrial control DJF values (U contour interval: 2 m/s) and stippled regions are statistically significant.

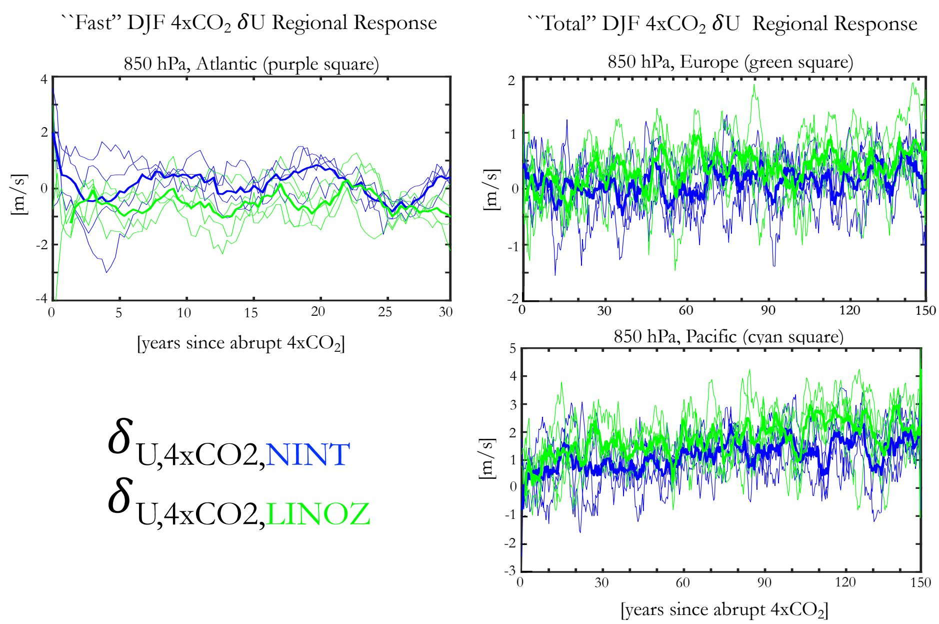


FIG. A3. Changes in the DJF zonal winds at 850 hPa, focusing on the "fast" (a) and "total" (b) responses to $4xCO_2$, relative to the preindustrial control simulations. The fast response is evaluated over the North Atlantic (50°W-10°W, 45°N-65°N). The slow response is evaluated over Europe (0°E-80°E, 45°N-65°N) and over the Pacific (150°E-150°W, 45°N-65°N). Results for the LINOZ and NINT ensembles are shown in green and blue, respectively (thick lines denote ensemble means).

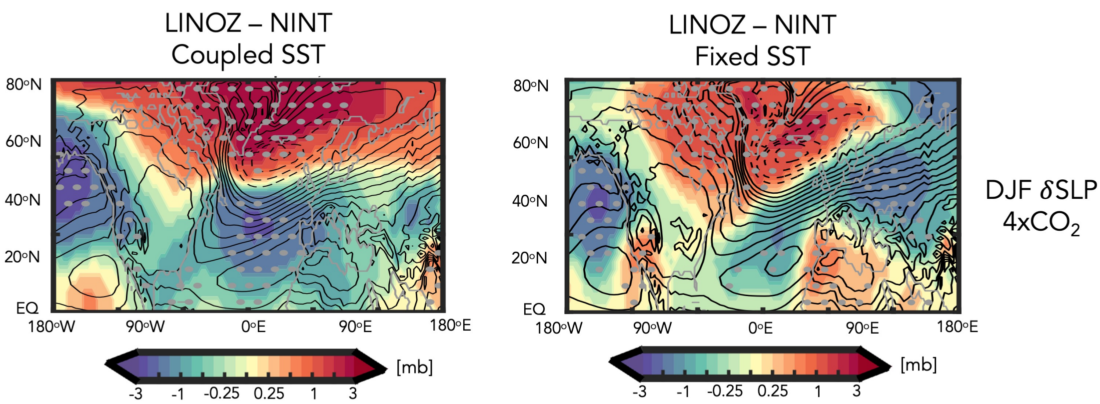


FIG. A4. Left panel: Colors show the LINOZ minus NINT ensemble mean difference in the December-January-February (DJF) "fast" response of the sea level pressure to an abrupt quadrupling of $CO_2$. Results are shown for the fully coupled atmosphere-ocean simulations. Right panel: The ensemble mean response in sea level pressure in the experiments in which the time-evolving 4x$CO_2$ ensemble mean LINOZ ozone response is prescribed and the SSTs, SICs, and background $CO_2$ are set to preindustrial values. Black contours denote climatological mean preindustrial control DJF values (contour interval: 10 mb). Stippled regions are statistically significant.

## References

Alexander, M. A., J. D. Scott, and C. Deser, 2000: Processes that influence sea surface temperature and ocean mixed layer depth variability in a coupled model. *Journal of Geophysical Research: Oceans*, **105 (C7)**, 16 823–16 842.

Ayarzagüena, B., and Coauthors, 2020: Uncertainty in the response of sudden stratospheric warmings and stratosphere-troposphere coupling to quadrupled $CO_2$ concentrations in CMIP6 models. *Journal of Geophysical Research: Atmospheres*, **125 (6)**, e2019JD032 345.

Baldwin, M. P., and Coauthors, 2021: Sudden stratospheric warmings. *Reviews of Geophysics*, **59 (1)**, e2020RG000 708.

Barnes, E. A., and L. Polvani, 2013: Response of the midlatitude jets, and of their variability, to increased greenhouse gases in the cmip5 models. *Journal of Climate*, **26 (18)**, 7117–7135.

Bauer, S. E., and Coauthors, 2020: Historical (1850–2014) aerosol evolution and role on climate forcing using the GISS ModelE2. 1 contribution to CMIP6. *Journal of Advances in Modeling Earth Systems*, **12 (8)**, e2019MS001 978.

Bellomo, K., M. Angeloni, S. Corti, and J. von Hardenberg, 2021: Future climate change shaped by inter-model differences in Atlantic meridional overturning circulation response. *Nature Communications*, **12 (1)**, 1–10.

Bellomo, K., V. L. Meccia, R. D'Agostino, F. Fabiano, S. M. Larson, J. von Hardenberg, and S. Corti, 2023: Impacts of a weakened amoc on precipitation over the euro-atlantic region in the ec-earth3 climate model. *Climate Dynamics*, 1–20.

Booth, B. B., N. J. Dunstone, P. R. Halloran, T. Andrews, and N. Bellouin, 2012: Aerosols implicated as a prime driver of twentieth-century North Atlantic climate variability. *Nature*, **484 (7393)**, 228–232.

Butler, A. H., D. W. Thompson, and R. Heikes, 2010: The steady-state atmospheric circulation response to climate change–like thermal forcings in a simple general circulation model. *Journal of Climate*, **23 (13)**, 3474–3496.

Ceppi, P., and D. L. Hartmann, 2015: Connections between clouds, radiation, and midlatitude dynamics: A review. *Current Climate Change Reports*, **1 (2)**, 94–102.

Ceppi, P., G. Zappa, T. G. Shepherd, and J. M. Gregory, 2018: Fast and slow components of the extratropical atmospheric circulation response to $CO_2$ forcing. *Journal of Climate*, **31 (3)**, 1091–1105.

Chiodo, G., and L. M. Polvani, 2019: The response of the ozone layer to quadrupled $CO_2$ concentrations: Implications for climate. *Journal of Climate*, **32 (22)**, 7629–7642.

Chiodo, G., L. M. Polvani, D. R. Marsh, A. Stenke, W. Ball, E. Rozanov, S. Muthers, and K. Tsigaridis, 2018: The response of the ozone layer to quadrupled $CO_2$ concentrations. *Journal of Climate*, **31 (10)**, 3893–3907.

Cowan, T., and W. Cai, 2013: The response of the large-scale ocean circulation to 20th century Asian and non-Asian aerosols. *Geophysical Research Letters*, **40 (11)**, 2761–2767.

DallaSanta, K., C. Orbe, D. Rind, L. Nazarenko, and J. Jonas, 2021a: Dynamical and trace gas responses of the quasi-biennial oscillation to increased $CO_2$. *Journal of Geophysical Research: Atmospheres*, **126 (6)**, e2020JD034 151.

DallaSanta, K., C. Orbe, D. Rind, L. Nazarenko, and J. Jonas, 2021b: Response of the quasi-biennial oscillation to historical volcanic eruptions. *Geophysical Research Letters*, **48 (20)**, e2021GL095 412.

Delworth, T. L., and K. W. Dixon, 2000: Implications of the recent trend in the Arctic/North Atlantic oscillation for the North Atlantic thermohaline circulation. *Journal of Climate*, **13 (21)**, 3721–3727.

Delworth, T. L., and F. Zeng, 2016: The impact of the North Atlantic oscillation on climate through its influence on the Atlantic meridional overturning circulation. *Journal of Climate*, **29 (3)**, 941–962.

Delworth, T. L., F. Zeng, L. Zhang, R. Zhang, G. A. Vecchi, and X. Yang, 2017: The central role of ocean dynamics in connecting the North Atlantic oscillation to the extratropical component of the Atlantic multidecadal oscillation. *Journal of Climate*, **30 (10)**, 3789–3805.

Eyring, V., S. Bony, G. A. Meehl, C. A. Senior, B. Stevens, R. J. Stouffer, and K. E. Taylor, 2016: Overview of the Coupled Model Intercomparison Project Phase 6 (CMIP6) experimental design and organization. *Geoscientific Model Development*, **9 (5)**, 1937–1958.

Garcia, R. R., and W. J. Randel, 2008: Acceleration of the Brewer–Dobson circulation due to increases in greenhouse gases. *Journal of the Atmospheric Sciences*, **65 (8)**, 2731–2739.

Gervais, M., J. Shaman, and Y. Kushnir, 2019: Impacts of the North Atlantic warming hole in future climate projections: Mean atmospheric circulation and the North Atlantic jet. *Journal of Climate*, **32 (10)**, 2673–2689.

Grise, K. M., and L. M. Polvani, 2014: The response of midlatitude jets to increased $CO_2$: Distinguishing the roles of sea surface temperature and direct radiative forcing. *Geophysical Research Letters*, **41 (19)**, 6863–6871.

Grise, K. M., and L. M. Polvani, 2016: Is climate sensitivity related to dynamical sensitivity? *Journal of Geophysical Research: Atmospheres*, **121 (10)**, 5159–5176.

Isaksen, I. S., and Coauthors, 2009: Atmospheric composition change: Climate–chemistry interactions. *Atmospheric Environment*, **43 (33)**, 5138–5192.

Jackson, L., R. Kahana, T. Graham, M. Ringer, T. Woollings, J. Mecking, and R. Wood, 2015: Global and european climate impacts of a slowdown of the amoc in a high resolution gcm. *Climate dynamics*, **45**, 3299–3316.

Jackson, L. C., and Coauthors, 2022: Understanding amoc stability: the north atlantic hosing model intercomparison project. *Geoscientific Model Development Discussions*, **2022**, 1–32.

Kantha, L. H., and C. A. Clayson, 2000: *Small scale processes in geophysical fluid flows*. Elsevier.

Kelley, M., and Coauthors, 2020: GISS-E2. 1: Configurations and climatology. *Journal of Advances in Modeling Earth Systems*, **12 (8)**, e2019MS002 025.

Khatri, H., R. G. Williams, T. Woollings, and D. M. Smith, 2022: Fast and slow subpolar ocean responses to the North Atlantic oscillation: Thermal and dynamical changes. *Geophysical Research Letters*, **49 (24)**, e2022GL101 480.

Li, F., and P. A. Newman, 2022: Prescribing stratospheric chemistry overestimates southern hemisphere climate change during austral spring in response to quadrupled $CO_2$. *Climate Dynamics*, 1–18.

Lindzen, R. S., 1987: On the development of the theory of the QBO. *Bulletin of the American Meteorological Society*, 329–337.

Liu, W., A. V. Fedorov, S.-P. Xie, and S. Hu, 2020: Climate impacts of a weakened Atlantic meridional overturning circulation in a warming climate. *Science Advances*, **6 (26)**, eaaz4876.

Ma, L., T. Woollings, R. G. Williams, D. Smith, and N. Dunstone, 2020: How does the winter jet stream affect surface temperature, heat flux, and sea ice in the North Atlantic? *Journal of Climate*, **33 (9)**, 3711–3730.

Marshall, J., H. Johnson, and J. Goodman, 2001: A study of the interaction of the North Atlantic oscillation with ocean circulation. *Journal of Climate*, **14 (7)**, 1399–1421.

McLinden, C., S. Olsen, B. Hannegan, O. Wild, M. Prather, and J. Sundet, 2000: Stratospheric ozone in 3-D models: A simple chemistry and the cross-tropopause flux. *Journal of Geophysical Research: Atmospheres*, **105 (D11)**, 14 653–14 665.

Meinshausen, M., and Coauthors, 2020: The shared socio-economic pathway (SSP) greenhouse gas concentrations and their extensions to 2500. *Geoscientific Model Development*, **13 (8)**, 3571–3605.

Menzel, M. E., D. Waugh, and K. Grise, 2019: Disconnect between hadley cell and subtropical jet variability and response to increased co2. *Geophysical Research Letters*, **46 (12)**, 7045–7053.

Meraner, K., S. Rast, and H. Schmidt, 2020: How useful is a linear ozone parameterization for global climate modeling? *Journal of Advances in Modeling Earth Systems*, **12 (4)**, e2019MS002 003.

Miller, R. L., and Coauthors, 2021: Cmip6 historical simulations (1850–2014) with GISS-E2. 1. *Journal of Advances in Modeling Earth Systems*, **13 (1)**, e2019MS002 034.

Mitevski, I., C. Orbe, R. Chemke, L. Nazarenko, and L. M. Polvani, 2021: Non-monotonic response of the climate system to abrupt $CO_2$ forcing. *Geophysical Research Letters*, **48 (6)**, e2020GL090 861.

Muthers, S., C. C. Raible, E. Rozanov, and T. F. Stocker, 2016: Response of the AMOC to reduced solar radiation–the modulating role of atmospheric chemistry. *Earth System Dynamics*, **7 (4)**, 877–892.

Nowack, P. J., N. Luke Abraham, A. C. Maycock, P. Braesicke, J. M. Gregory, M. M. Joshi, A. Osprey, and J. A. Pyle, 2015: A large ozone-circulation feedback and its implications for global warming assessments. *Nature Climate Change*, **5 (1)**, 41–45.

O'Callaghan, A., M. Joshi, D. Stevens, and D. Mitchell, 2014: The effects of different sudden stratospheric warming types on the ocean. *Geophysical Research Letters*, **41 (21)**, 7739–7745.

Orbe, C., and Coauthors, 2020: GISS Model E2.2: A climate model optimized for the middle atmosphere—2. Validation of large-scale transport and evaluation of climate response. *Journal of Geophysical Research: Atmospheres*, **125 (24)**, e2020JD033 151.

Orbe, C., and Coauthors, 2023: Atmospheric response to a collapse of the north atlantic circulation under a mid-range future climate scenario: A regime shift in northern hemisphere dynamics. *Journal of Climate*, 1–52.

Reichler, T., J. Kim, E. Manzini, and J. Kröger, 2012: A stratospheric connection to Atlantic climate variability. *Nature Geoscience*, **5 (11)**, 783–787.

Rind, D., J. Jonas, N. Balachandran, G. A. Schmidt, and J. Lean, 2014: The QBO in two GISS global climate models: 1. Generation of the QBO. *Journal of Geophysical Research: Atmospheres*, **119 (14)**, 8798–8824.

Rind, D., G. A. Schmidt, J. Jonas, R. Miller, L. Nazarenko, M. Kelley, and J. Romanski, 2018: Multicentury instability of the Atlantic meridional circulation in rapid warming simulations with GISS ModelE2. *Journal of Geophysical Research: Atmospheres*, **123 (12)**, 6331–6355.

Rind, D., R. Suozzo, N. Balachandran, A. Lacis, and G. Russell, 1988: The GISS global climate-middle atmosphere model. Part I: Model structure and climatology. *Journal of the Atmospheric Sciences*, **45 (3)**, 329–370.

Rind, D., and Coauthors, 2020: GISS Model E2.2: A climate model optimized for the middle atmosphere—model structure, climatology, variability, and climate sensitivity. *Journal of Geophysical Research: Atmospheres*, **125 (10)**, e2019JD032 204.

Roach, L. A., E. Blanchard-Wrigglesworth, S. Ragen, W. Cheng, K. C. Armour, and C. M. Bitz, 2022: The impact of winds on AMOC in a fully-coupled climate model. *Geophysical Research Letters*, e2022GL101203.

Robson, J., and Coauthors, 2022: The role of anthropogenic aerosol forcing in the 1850–1985 strengthening of the amoc in cmip6 historical simulations. *Journal of Climate*, **35 (20)**, 6843–6863.

Romanou, A., and Coauthors, 2023: Stochastic bifurcation of the North Atlantic circulation under a mid-range future climate scenario with the NASA-GISS ModelE. *Journal of Climate*.

Shaw, T., and Coauthors, 2016: Storm track processes and the opposing influences of climate change. *Nature Geoscience*, **9 (9)**, 656–664.

Shaw, T. A., 2019: Mechanisms of future predicted changes in the zonal mean mid-latitude circulation. *Current Climate Change Reports*, **5 (4)**, 345–357.

Shepherd, T. G., 2014: Atmospheric circulation as a source of uncertainty in climate change projections. *Nature Geoscience*, **7 (10)**, 703–708.

Sigmond, M., and J. F. Scinocca, 2010: The influence of the basic state on the Northern Hemisphere circulation response to climate change. *Journal of Climate*, **23 (6)**, 1434–1446.

Simpson, I. R., T. A. Shaw, and R. Seager, 2014: A diagnosis of the seasonally and longitudinally varying midlatitude circulation response to global warming. *Journal of the Atmospheric Sciences*, **71 (7)**, 2489–2515.

Smith, D. M., and Coauthors, 2019: The polar amplification model intercomparison project (PAMIP) contribution to CMIP6: Investigating the causes and consequences of polar amplification. *Geoscientific Model Development*, **12 (3)**, 1139–1164.

Swingedouw, D., P. Ortega, J. Mignot, E. Guilyardi, V. Masson-Delmotte, P. G. Butler, M. Khodri, and R. Séférian, 2015: Bidecadal North Atlantic ocean circulation variability controlled by timing of volcanic eruptions. *Nature Communications*, **6 (1)**, 1–12.

Vallis, G. K., P. Zurita-Gotor, C. Cairns, and J. Kidston, 2015: Response of the large-scale structure of the atmosphere to global warming. *Quarterly Journal of the Royal Meteorological Society*, **141 (690)**, 1479–1501.

Visbeck, M., H. Cullen, G. Krahmann, and N. Naik, 1998: An ocean model's response to North Atlantic oscillation-like wind forcing. *Geophysical Research Letters*, **25 (24)**, 4521–4524.

Voigt, A., and T. A. Shaw, 2015: Circulation response to warming shaped by radiative changes of clouds and water vapour. *Nature Geoscience*, **8 (2)**, 102–106.

Yuval, J., and Y. Kaspi, 2020: Eddy activity response to global warming–like temperature changes. *Journal of Climate*, **33 (4)**, 1381–1404.

Zhai, X., H. L. Johnson, and D. P. Marshall, 2014: A simple model of the response of the Atlantic to the North Atlantic oscillation. *Journal of Climate*, **27 (11)**, 4052–4069.

Zhang, R., R. Sutton, G. Danabasoglu, Y.-O. Kwon, R. Marsh, S. G. Yeager, D. E. Amrhein, and C. M. Little, 2019: A review of the role of the atlantic meridional overturning circulation in atlantic multidecadal variability and associated climate impacts. *Reviews of Geophysics*, **57 (2)**, 316–375.

Zhang, R., and Coauthors, 2013: Have aerosols caused the observed atlantic multidecadal variability? *Journal of the Atmospheric Sciences*, **70 (4)**, 1135–1144.

Zhang, X., D. W. Waugh, and C. Orbe, 2023: Dependence of northern hemisphere tropospheric transport on the midlatitude jet under abrupt co2 increase. *Journal of Geophysical Research: Atmospheres*, e2022JD038454.